Spike substitution T813S increases Sarbecovirus fusogenicity by enhancing the usage of TMPRSS2

Yong Ma[1¶], Pengbin Li[1¶], Yunqi Hu[1¶], Tianyi Qiu[2], Lixiang Wang[5], Hongjie Lu[1], Kexin Lv[1], Mengxin Xu[1], Jiaxin Zhuang[3], Xue Liu[3], Suhua He[7], Bing He[1], Shuning Liu[1], Lin Liu[1], Yuanyuan Wang[1], Xinyu Yue[1], Yanmei Zhai[1], Wanyu Luo[1], Haoting Mai[1], Wenjing Zhao[3], Jun Chen[5], Shoudeng Chen[7],Xiaoli Xiong[4], Mang Shi[3], Ji-An Pan[3,*] and Yao-Qing Chen[1,6,*]

1 School of Public Health (Shenzhen), Sun Yat-sen University, Shenzhen, Guangdong Province, China, **2** Institute of Clinical Science, Zhongshan Hospital, Shanghai Medical College, Fudan University, Shanghai, China, **3** The Center for Infection and Immunity Study and Molecular Cancer Research Center, School of Medicine, Shenzhen Campus of Sun Yat-sen University, Shenzhen, Guangdong Province, China, **4** State Key Laboratory of Respiratory Disease, CAS Key Laboratory of Regenerative Biology, Guangdong Provincial Key Laboratory of Stem Cell and Regenerative Medicine, Guangzhou Institutes of Biomedicine and Health, Chinese Academy of Sciences, Guangzhou, Guangdong Province, China, **5** Department of Immunology and Microbiology, Zhongshan School of Medicine, Sun Yat-sen University, Guangzhou, Guangdong Province, China, **6** National Medical Products Administration Key Laboratory for Quality Monitoring and Evaluation of Vaccines and Biological Products，Sun Yat-sen University, Guanzhou, Guangdong Province, China, **7** Molecular Imaging Center, Guangdong Provincial Key Laboratory of Biomedical Imaging, the Fifth Affiliated Hospital, Sun Yat-sen University, Zhuhai, Guangdong Province, China

¶ These authors contributed equally to this work

* panjan@mail.sysu.edu.cn (JAP); chenyaoqing@mail.sysu.edu.cn (YQC)

Abstract

SARS-CoV Spike (S) protein shares considerable homology with SARS-CoV-2 S, especially in the conserved S2 subunit (S2). S protein mediates coronavirus receptor binding and membrane fusion, and the latter activity can greatly influence coronavirus infection. We observed that SARS-CoV S is less effective in inducing membrane fusion compared with SARS-CoV-2 S. We identify that S813T mutation is sufficient in S2 interfering with the cleavage of SARS-CoV-2 S by TMPRSS2, reducing spike fusogenicity and pseudoparticle entry. Conversely, the mutation of T813S in SARS-CoV S increased fusion ability and viral replication. Our data suggested that residue 813 in the S was critical for the proteolytic activation, and the change from threonine to Serine at 813 position might be an evolutionary feature adopted by SARS-2-related viruses. This finding deepened the understanding of Spike fusogenicity and could provide a new perspective for exploring *Sarbecovirus*' evolution.

Author Summary

The Spike strain of SARS-CoV-2 has accumulated many mutations during its time in circulation, most of which have occurred in the S1 region, and more specifically in the RBD, in an effort to either improve the virus's affinity for the receptor ACE2 or to

enhance its ability to evade the immune system. Mutations in the Spike S2 region have more far-reaching effects than those in the S1 region because it is more conserved across sarbecoviruses. By comparing SARS and SARS2, we found that an important substitution at amino acid position 813 in the S2 region (T813S) disrupts the utilization of TMPRSS2 and can significantly influence viral entry into cells. This discovery deepens our knowledge of S proteins and provides new prospects for tracing the evolution of Sarbecoviruses.

Introduction

Since its outbreak, SARS-CoV-2 (SARS2) has caused hundreds of millions of illnesses and fatalities globally, making it by far the worst public health catastrophe of the 21st century [1]. SARS2 was the seventh human coronavirus and likely originated in a bat host [2,3], belonging to the Sarbecovirus subgenus of betacoronavirus [4,5], along with SARS-CoV (SARS), which caused an outbreak in 2002-2003 [6]. Spike (S), as the surface glycoprotein, facilitates virus' cell entry through host receptor binding with its S1 subunit (S1) and membrane fusion mediated by its S2 subunit (S2) [7,8]. The receptor-binding domain (RBD) is located towards the C-terminus of S1 and is responsible for binding to the receptor, angiotensin-converting enzyme 2 (ACE2) [9,10]. RBD is the primary focus of vaccine designing [11-13] and neutralizing antibody screening [14-16] despite being highly genetically variable among variants [17-19]. After spike binding to ACE2, conformational change of S2 is triggered and this

conformational change facilitates fusion between the viral and host cell membranes [20], this process is believed to be highly modulated by proteolysis.

Spike protein contains multiple proteolytic sites, while a single arginine is usually located at the S1/S2 boundary and susceptible to trypsin-like protease cleavage. It is unique among Sarbecovirus spikes that SARS2 S contains a multi-basic cleavage site (681-PRRA-684), between the S1 and S2 subunits [21]. It has been proposed that cleavage at the S1/S2 site facilitates S priming and promotes membrane fusion but is not essential to membrane fusion [22]. Spike S2 contains a S2' site for cellular protease cleavage [23,24]. It has been proposed that the S2' site must be cleaved to fully initiate the fusion process, by either transmembrane serine protease 2 (TMPRSS2) [25] on the cell surface or by cathepsin L (CTSL) [26] in the endosomes. S2 consisted of 3 key motifs for membrane fusion: fusion peptides (FPs) and heptad repeat 1 (HR1) and 2 (HR2). HR1 and HR2 form a six-helix bundle fusion core in post-fusion S [27]. FPs are pivotal in viral entry and highly conserved between β-coronaviruses [23]. However, the exact sequence of "fusion peptide" has not yet been determined [28-31]. In a previous study, two FP candidates have been identified based on cleavage sites [28], FP1 (Animo acid (AA) 788-806) located behind S1/S2 and the extremely conserved FP2 (AA815-833) located behind S2' site.

The membrane fusion process is crucial to viral infection. Despite sharing about 76.47% amino acid identity on S protein [32], SARS and SARS2 have generated extremely distinct infection events: The SARS-CoV-2 pandemic has lasted for more than three years and the virus is likely to remain circulating. In contrast, the 2003

SARS-CoV world-wide outbreak was quickly eradicated. The exact reason for the transmissibility difference between the two related viruses is likely to be complex and yet to be understood. The ability to use ACE2 efficiently has been proposed to be a key prerequisite for viral infection [33]. It has been reported that SARS2 S binds to ACE2 with 10- to 20-fold higher affinity than SARS S [34], but another research showed similar affinities between SARS and SARS2 RBD binding with ACE2 [35]. Although receptor binding is an essential step for virus cell entry, the subsequent S2 mediated membrane fusion is also essential [36]. In this study, we investigated the fusogenic activities of S2 using a split-GFP system, and we found that SARS2 S2 mediates more robust membrane fusion than SARS S2. We further demonstrated that the threonine to serine substitution at residue 813 in S2 significantly enhance membrane fusion and probably enhance the spread of *Sarbecovirus*.

Results

SARS2 S2 induced more syncytia formation than SARS S2

To investigate the role of S2 in SARS2 infection, we constructed a chimera SARS2-S protein bearing SARS S2 (cSARS2-S2sars, spike2), and a chimera SARS-S protein bearing SARS2 S2 (cSARS-S2sars2, spike4) (Fig 1A). Fluorescence-activated cell sorting (FACS) experiments showed that the surface expression levels were the same between the chimeric S and their parents (Figs 1B and 1C). Western blot (WB) analysis showed no significant difference in cleavage efficiency between chimeric S and their parents with or without trypsin (Fig 1D). However, we found that the cleavage

111 efficiency of SARS2 S was higher than that of SARS S, and trypsin treatment increased
112 the cleavage of SARS S significantly (Fig 1D). In the following membrane fusion
113 assays, we treated all S proteins expressed on cells with trypsin.

114 To assay the membrane fusion activities of these chimeric S proteins, we utilized
115 a green fluorescent protein (GFP)–Split complementation system [37, 38], in which
116 GFP is split into two non-fluorescent parts, GFP1-10 and GFP11, and the reassembly
117 of GFP1-10 and GFP11 reconstitutes a functional chromophore. With transfection, we
118 introduced GFP1-10 and GFP11 into the donor cells transiently expressing various S
119 proteins and the acceptor cells stably expressing ACE2 (hACE2) and TMPRSS2,
120 respectively. The spike-mediated fusion of donor and acceptor cells could lead to the
121 formation of syncytia. Thus, GFP1-10 and GFP11 were present in the same intracellular
122 environment and formed a functional chromophore. The fluorescence from the
123 chromophore reflects the fusion activities of these S proteins (Fig 1F). Two hours after
124 the coculture of donor and acceptor cells, the cell fusion accompanied by the GFP was
125 observed under microscopy, and the green fluorescence positive area increased rapidly
126 with more cell fusion (Fig 1E). In this work, we quantified cell fusion activity by
127 calculating the area ratio of GFP to DAPI. We observed that the rate and size of
128 syncytium formation were affected by various S proteins. SARS2-S was more effective
129 at cell fusion than SARS-S, which is consistent with their spread ability. Of note, we
130 found the cell fusion ability of S proteins were mainly correlated with the S2. When
131 replaced with SARS2 S2, the fusogenicity of chimeric protein cSARS-S2sars2 was
132 remarkably improved compared with its parent, SARS; the fusion rate and size all

133 increased; on the other side, after replacing SARS S2, the chimera S protein cSARS2-
134 S2sars lost most of its cell fusion ability, the fusion rate and size reduced significantly
135 (Figs 1E and 1G).

136 Collectively, these results suggest that S2 plays an important role in SARS2
137 infection, and its alternation it could affect the fusogenicity of S protein significantly.

138

139 The Spike fusogenicity is dependent on the Internal Fusion Peptide
140 (IFP)

141 To further identify key functional domains or motifs in S2 for increased spike
142 fusogenicity, we divided S2 into three parts based on their functions [23, 39] and
143 constructed chimeric Spike5 (SARS F1, AA668-816), Spike6 (SARS F2, AA817-966),
144 Spike7 (SARS F3, AA967-1214) and Spike10 (SARS2 F1, AA686-833), Spike11
145 (SARS2 F2, AA834-984), Spike12 (SARS2 F3, AA985-1213) by directly replacing
146 amino acids of the corresponding regions on Spike1 and Spike3, respectively, as shown
147 in Figs 2A and 2G. Via FACS and WB assay, we confirmed no significant difference
148 in cell surface expression of these S proteins (Figs 2B and 2H); and the unchanged
149 CL-S ratio for most chimera S, except for Spike 6, with increased cleavage; and Spike
150 5, with decreased cleavage (Figs 2C and 2D). Subsequent membrane fusion assays
151 showed that swapping of F1 regions significantly affected the fusogenicity of the
152 chimeric S proteins. The area of GFP decreased after introducing SARS F1 into
153 SARS2-S (Spike 5, Figs 2E and 2F), while GFP signal increased significantly when
154 SARS2 F1 was introduced into SARS1-S (Spike 10, Figs 2K and 2L). The swapping

of F2 and F3 between SARS-S and SARS2-S failed to produce a similar significant alternation in the fusogenicity of S proteins as F1.

We further divided F1 into two portions based on whether they contained FPs or not. We define the Non-Fusion Peptide (NFP) fragment at the N-terminus and the Internal Fusion Peptide (IFP) fragment at the C-terminus. IFP fragment contained FP1 and FP2. Following the similar abovementioned strategy for swapping mutant S proteins, we constructed following chimeric S constructs. We found that after swapping NFP (Spike8, SARS AA668-769; Spike13, SARS2 AA686-787) and IFP (Spike9, SARS AA770-816; Spike14, SARS2 AA788-833), the surface expression of chimeric S was the same as the parents (Spike1 and Spike3) (Figs 2B and 2H), while the cleavage ability had a difference. We found that introducing SARS IFP into SARS2-S and introducing SARS2 NFP into SARS-S could affect the expression of S protein and decreased spike cleavage respectively (Figs 2C and 2D; Figs 2I and 2J), these results suggested direct motif replacement might affect the cleavage of S, and SARS2 FP, especially IFP, might enhance the ratio of CL-S. Subsequent membrane fusion assays showed that IFP was the key factor of S fusogenicity, replacing SARS IFP alone to SARS2 backbone (Spike9) was able to reduce S protein's membrane fusion capacity significantly and vice versa (Spike14) (Figs 2E and 2F, Figs 2K and 2L). We also found that SARS2 F2 fragment (Spike 11) promoted fusion and this might be related to the increased S expression.

To further validate the role of IFP in S fusogenictiy, we directly replaced fragments on Spike2 and 4 for chimeric plasmid construction (S1 Figs A and F) and further

assayed cell membrane fusion ability. We found that the surface expression (S1 Figs C and H) and the CL-S ratio (S1 Figs B and G) of most chimera S was the same, except for the reduction in Spike20 and the enhancement of Spike19 and 22 (S1 Figs B and G), this results further proved SARS2 IFP enhanced the cleavage of S protein. The membrane fusion results showed that introducing SARS2 F1 or IFP moderately enhanced the fusion ability of Spike2 (S1 Figs D and E), but substitution of SARS F1 and IFP significantly inhibited the fusion ability of Spike4 (S1 Figs I and J), these results confirmed that the backbone of chimeric protein might affect S fusogenicity, but IFP was the importance.

Collectively, these results showed that although there was some variation across chimera S, IFP was the most critical factor affecting fusion.

IFP S813T mutation reduced the cell membrane fusion ability of SARS-CoV-2 S protein significantly.

The IFP sequence is relatively conserved between SARS S and SARS2 S, with only six different amino acid. To investigate whether these amino acids influence the fusogenicity of S protein, we investigated the impact of each amino acid on cell membrane fusion by introducing mutations on each of them in Spike9 (Figs 3A and 3F). WB and FACS assays revealed no significant differences in expression and cleavage of each mutant S protein, except for Spike29, which is poorly expressed (Figs 3B and 3C). Subsequent membrane fusion assays revealed that only the T813S mutation significantly increased the chimeric protein's fusion capability (Figs 3D and 3E).

Similar experiments were performed on Spike14. The expressions and cleavages of all mutant, Spike31-36, were comparable to that of the parent S protein, spike14 (Figs 3G and 3H). Despite Spike31 (I788M) and Spike32 (P793T) showing mildly reduced fusion activities, subsequent experiments showed that only the S813T mutation reduced the membrane fusion properties of the S protein significantly (Figs 3I and 3J). These findings corroborated that the mutation of serine to threonine on residue 813 dramatically reduced the fusion ability of chimeric S proteins, suggesting that residue 813 plays a pivotal role in SARS and SARS2 S2 mediated-fusogenicity.

S813T mutation disturbed the *Sarbecovirus*'s membrane fusion and infection significantly.

To further consolidate the above findings, we introduced S813T mutation in S proteins of SARS2 and its variants of concern (VOC) strains (Spike37-41), and T813S mutation in that of SARS. As shown in Figs 4A and 4B, the membrane fusion activities of spikes with S813 were significantly higher than those spikes with T813 in both ACE2-293T and Caco2 cells, and this trend was independent of the native membrane fusion capability of the S protein. The FACS assay confirmed no significant difference in the expression of various S proteins. Even though the levels of S protein cleavage varied between strains, S813 and T813 S proteins of the same strain had roughly the same level of cleavage, with only S813 S proteins of SARS2 and Delta, T813 S protein of SARS having noticeably stronger levels of cleavage than their counterparts. As a result

of this finding, it appeared that the promotion of S813 on membrane fusion originated from a mechanism independent of S1/S2 cleavage.

Considering the pivotal role of S813 in the membrane fusion properties of the S protein, we next interrogated S813 for its possible role in viral infection. We rescued single-cycle infectious SARS viruses by coexpressing the SARS2 replicon [68] and various S genes in package cells. The viruses with various S proteins were used to infect ACE2-293T and Caco2, and the replication products, subgenomic RNAs, were quantified with RT-qPCR. As shown in Fig 4E, the transduction activity of the mutant with S813 S was significantly higher than that of T813 S in SARS2, SARS, or VOC strains. These results indicated that S813T can affect virus entry by modulating the membrane fusion properties of S protein.

The S813T mutation has no effect on S protein interactions with ACE2.

To investigate how S813T mutation alters S fusogenicity, we used a competitive ELISA assay to examine the role of residue 813 in interactions between S protein and ACE2. S813 S and T813 S was separately expressed firstly (Figs 6A). In our study, SARS2 S contained six proline substitutions to generate stabilized and soluble prefusion form [40-42]; SARS S also contained two stabilizing proline mutations in S2 subunit according to an effective stabilization strategy [43, 44]. The results showed that S813 S and T813 S proteins had similar affinities towards the ACE2 receptor, indicating that S813T mutation had no effect on S protein receptor binding (Fig 6B). We further verified this finding by assessing the neutralization of RBM-targeting antibodies, which

242 directly blocked the interaction between S protein and ACE2. In this study, we used
243 antibody m396 [45] for SARS, and X65 [15] for SARS2; we found that the
244 representative antibodies showed similar neutralization efficiencies against VSV
245 particles pseudotyped (VSVpp) with parental and mutant S proteins (Fig 5C). In
246 summary, we confirmed that the S813T mutation did not affect S protein interactions
247 with ACE2 and RBD antibodies.
248
249 **S813T mutation reduced the use of TMPRSS2 by S protein.**
250 Proteolytic activation of S is critical in the process of CoV entry into cells [46]. It has
251 been reported that efficient infection of SARS and SARS2 requires sequential cleavage
252 of S by furin at the S1/S2 site and then by TMPRSS2 at the S2' site or by CTSL at two
253 specific sites [47] in endosome when TMPRSS2 expression is repressed (Fig 6A). We
254 noticed that S2' site is highly conserved in *Sarbecovirus* spikes and residue 813 is
255 located in close proximity to the S2' site, highly conserved in *Sarbecovirus* spikes, and
256 therefore the 813 change could potentially affect cleavage by TMPRSS2.
257 To test this hypothesis, we investigated the impact of S813T mutation on the S2'
258 site cleavage of spike on VSVpp. WB analyses showed that S813T mutation had the
259 most significant effect on S2' cleavage compared with other point mutations in IFP (Fig
260 6B). At the same time, we overexpressed TMPRSS2 in ACE2-293T cells firstly (S2
261 Fig C) and then used the GFP-split system to compare the fusion activities of S813 S
262 and T813 S. We found membrane fusion activities of S813 S and T813 S increased with
263 increasing level of TMPRSS2 expression and both plateaued to similar levels (S2 Figs

A and B), this phenomenon was observed for most VOC strains, with only Delta S813 S being stronger than T813 S (Figs 6C and 6D), indicating that increasing TMPRSS2 expression restored the S813T mutation to interfere with S proteins, in other words, the S813T mutation likely reduced S protein sensitivity to TMPRSS2.

To further investigate this possibility, we used the TMPRSS2-specific inhibitor Camostat and examined its effect on membrane fusion under various concentrations, the results (Figs 6E-6G) show that when Camostat concentration was low (10 μM), there was no discernible difference in the ability of S813 S and T813 S in the ACE2-293T/TMPRSS2 system; however, when the Camostat concentration was increased, the difference gradually became apparent, eventually showing that S813 S was significantly higher than T813 S (Figs 6E and 6F). The effect of CTSL inhibitor E-64d was also tested and the results revealed that it had a modest, concentration-independent inhibitory effect in the ACE2-293T/TMPRSS2 system, but did not affect the fusion ability between S813 S and T813 S, suggesting the effect of CTSL on S protein activation was diminished in the presence of TMPRSS2.

Based on these results, it is suggested that the S813T mutation has an effect on S protein fusion pathway modulated by TMPRSS2 by reducing TMPRSS2 cleavage at the S2' site. S813 S protein had higher utilization and could complete cleavage under lower TMPRSS2 conditions; whereas the T813 S protein used lower and required increased amounts of TMPRSS2 to complete cleavage.

Evolution AA 813 on Spike in *Sarbecovirus*.

Considering the significance of residue 813 in the S protein activation process, we reconstructed an evolutionary tree using the S protein sequences of representative SARS, SARS2 and SARS-relative (SARSr) strains to observe their evolutionary trends in *Sarbecovirus*. At position 813, we observed mostly threonine and serine; threonine was almost only present in two major lineages of SARSr strains, including human SARS-CoV and related viruses; while serine was found in human SARS-CoV-2 strains, bat and pangoline associated SARS-like strains related to SARS2 (such as RaTG13 discovered in 2013 and SL-CoVZXC21 discovered in 2015), as well as a lineage basal to all members of *Sarbecovirus* (Fig 7A). Meanwhile, the mutation frequency of the amino acid at position 813 was calculated with 114 unique SARSr sequences and 10060583 unique SARS2 sequences (GISAID 2020-2022.5.31), respectively. We discovered that in SARS, T813 accounted for 96.49% of the total and S813 accounted for 2.63%; however, in SARS2, S813 accounted for as higher as 99.9%, while T813 accounted for only 0.01% (Fig 7B). Therefore, for SARS-CoV-2 T813 S was likely to be a random mutation that occurred in only a few individuals, without major sustained circulation in human population. Intriguingly, we discovered that other than SARS-CoV and related viruses, the rest of the β-cov, which included highly pathogenic MERS-CoV and SARS2, and the less pathogenic OC43-CoV and HKU1-CoV, were all predominantly serine (Fig 7C).

Discussion

Previous research has proposed that ACE2 binding efficiency [34] and polybasic cleavage site "RRAR" at S1/S2 boundary [31,48] were the primary causes. SARS and SARS2 recognized the same receptor- ACE2 in Humans. The previous study has shown that mutations in the SARS2 RBD make it more accessible to the N-terminal end of ACE2 and stabilize two virus-binding hotspots at SARS2 RBD/ACE2 interface [49]. The polybasic cleavage site of SARS2 has been demonstrated to act as a determinant of transmission [50]. Studies found that the site sensitized SARS2 S protein to fusion-activating proteolysis during virus-cell entry [51]. In this study, we examined the membrane fusion activity of chimeric proteins with various S2s. Our results showed that the activity of S proteins bearing SARS2 S2 is significantly higher than that bearing SARS S2, suggesting that alternation of S2 is sufficient to change the membrane fusion activity of S proteins without disturbing the RBD/ACE2 interaction. We narrowed down the functional domains of S2 to IFP, which is essential for the membrane fusion activity of S protein. Furthermore, we identified the key residue serine 813, as indicated by the data that a single mutation of T813S in SARS S protein could enhance membrane fusion in cell-based membrane fusion assays and viral entry in a single-cycle infectious SARS virus system.

Residue 813 is located immediately upstream of S2' site (Figure 3A & 3F) and is conserved in various coronavirus strains (Figure. 7C). A recent study proposed that the replication-competent VSVΔG-SARS2 S would especially harbor the S813Y mutation, which reduced the enzymatic activity of TMPRSS2 and increased the stability of S protein for better vaccine design [52]. This unexpected discovery was in agreement

with our finding and highlighted the importance of S813 in S protein fusion activity. However, it should be noted that S813Y mutation is not observed in known viral genomic sequences. In contrast, S813 and T813 used in our study are from the SARS2 and SARS sequences, respectively. Thus, our findings were relevant to understanding the real function role of residue 813 during viral entry into the cell.

Host proteases, including furin, TMPRSS2, and CTSL work together to modulate coronavirus S protein-mediated cell fusion [53]. TMPRSS2 is a type Ⅱ transmembrane protein with serine protease activity and is required to trigger cell-cell fusion, it has been reported that TMPRSS2 knock-out 293T cells are unable to form syncytia [54]. TMPRSS2 has been proved to have stronger proteolytic activity against SARS2 S than SARS S. A study has shown that this is due to the multibasic site at S1/S2 boundary, when introduced it into SARS S or ablated it from SARS2 S, the difference can be diminished [36,55]. Here we found that the S2 also affected the utilization of TMPRSS2, the cleavage activity of TMPRSS2 on S813 S was significantly higher than that of T813 S in both SARS and SARS2, and the effect of S813T mutation decreased with increased TMPRSS2 expression. Our data suggested that residue 813, in addition to the multibasic site at S1/S2, could somewhat affect the activity of TMPRSS2 on S protein.

Our study demonstrated that S813T mutation affect the usage of TMPRSS2, did residue 813 impact the function of Furin and CTSL? Furin is ubiquitously expressed in cells [56] and for SARS-CoV-2 S the cleavage site is located in the S1/S2 boundary [54]. Recently, a study found that K814A mutation significantly reduced furin-

mediated cleavage of SARS2 S and antagonized pseudovirus transduction, while the S813A had no effect [57]. This work suggests that residue 813 is unlikely to affect furin cleavage. CTSL is a member of the lysosomal cysteine protease and was highly expressed in most human tissues, including the respiratory system, gastrointestinal tract, kidney, and urogenital system [58]. Previous studies have shown that CTSL played a role in the proteolysis of SARS S [59,60] and SARS2 S [26], and the cleavage site of CTSL in SARS S was at (near) S1/S2 [59], while in SARS2 S, it was at two distinct conserved locations in the S1 subunit [47], suggesting residue 813 did not affect CTSL cleavage.

SARS-CoV-2 is a fast-evolving virus, with rapid nucleotide substitution and recombination to generate new strains of altered virulence [61]. A most well-known example was the SARS2 D614G strain rapidly replaced the original virus strain and became the dominant variant [62]. Further studies showed that D614G substitution favored an open conformational state of S protein [63] and promoted syncytium formation through enhanced furin-mediated S cleavage [64]. Through phylogenetic analysis of representative Sarbecovirus S sequences from SARS outbreak in 2002 to the emergence of COVID19 in 2022, we determined that threonine and serine are the only two potential amino acids at position 813 in Sarbecovirus, however, T813S mutation enhanced the S protein membrane fusion function, which might be likely leading to the emergence of SARS-CoV-2 in nature.

In summary, our study demonstrated that residue 813 was a key determinant of S protein fusogenicity and infectivity. The selection and increasing frequency of S813 S

following the evolution of Sarbecovirus suggested that the T813S mutation was associated with an improvement of viral fitness through an increased S protein processing and fusogenic potential. These findings have important implications for understanding of the viral S fusogenicity.

Materials and methods

Cells and agents

Human embryonic kidney 293T (HEK293T) cells were maintained in Dulbecco's modified Eagle's medium (DMEM, Gibco) supplemented with 10% fetal bovine serum (FBS), 100 units/ml penicillin, 100 μg/ml streptomycin, and 2 mM L-glutamine. HEK293T cells that stably express human ACE2 (ACE2-293T) were cultivated in the presence of 2 μg/ml puromycin (Invivogen). Caco2 (human epithelial colorectal adenocarcinoma) cells were cultivated in DMEM (Gibco) containing 20% FBS (TransGen Biotech), 100 μg/ml streptomycin (biosharp), 100 U/ml penicillin (biosharp), 1 mM Non-essential amino acids (NEAA, Gibco). All Cell cultures were incubated at 37°C and 5% CO_2.

Plasmids

The pcDNA3.1(+) plasmid backbone was appended with a FLAG-tag sequence (DYKDDDDK) at the C-terminal. The spike coding sequences were all codon optimized for human cells. For the construction of recombinant S plasmids. S2 subunit

394 of SARS-CoV and SARS-CoV-2 VOC strains were amplified by PCR and appended
395 with other regions of the target spike backbone to facilitate In-Fusion cloning.
396 pQCXIP-BSR-GFP11 and pQCXIP-GFP1-10 were from Addgene (68715,68716);
397 Human TMPRSS2 was amplified from Caco2 cells and cloned into pcDNA3.1(+) with
398 a C-terminal FLAG-tag. All DNA constructs were verified by Sanger sequencing
399 (ACGT).
400

401 ## Fluorescence-activated cell sorting (FACS)

402 We conducted FACS using a Beckman CytExpert (Beckman) and data was analyzed
403 with FlowJo software. 293T cells transfected with S proteins for 36h were performed
404 in PBS with 1% BSA. Cells were incubated with primary antibodies on ice for 1h and
405 washed twice with PBS, then incubated with FITC goat anti-human IgG(H+L)
406 (Southern Biotechnology Associates,1:400) for 45 min on ice. Transfection efficiency
407 was assessed by staining with SARS-CoV-2 RBD specific antibodies: s309 [65]
408 (sotrovimab), which had been proved to pan-bind with SARS-CoV-2 VOC strains.
409

410 ## Western blot analysis

411 Western blot analysis was performed as previously described procedures [66]. Briefly,
412 cells were washed with ice-cold PBS and soluble proteins were extracted with cell lysis
413 buffer (100mM Tris-HCl pH=8.0, 150mM NaCl, 1% NP-40, phosphatase and protease
414 inhibitor cocktail tablets (Abcam)) according to the manufacturer's protocol. For the
415 analysis of S protein processing in VSV pseudotyped particles (VSVpp), we loaded 10

ml VSVpp onto 500 µl of a 20% (w/v) sucrose cushion and performed high-speed centrifugation (25000 g for 120 min at 4℃), the concentrated particles were re-suspended in 50 µl PBS. Equal amounts of protein samples were separated by 8% sodium dodecyl sulfate-polyacrylamide gel electrophoresis (SDS-PAGE) and transferred to nitrocellulose filter (NC) membranes. Mouse monoclonal antibodies targeting FLAG tag, β-actin (TransGen Biotech, 1:5000) were used as primary antibodies, horseradish peroxidase-conjugated (HPR) goat anti-mouse IgG antibody (Southern Biotechnology Associate, 1:10000) was the second antibody. The quantitative result of the ratio of cleaved to a full-length spike in immunoblots was analyzed by Image J software.

Fusion assay

This assay utilized a dual split protein (DSP) encoding the GFP gene, and the respective split proteins, DSP1-10 and DSP11, were expressed in effector and target cells by transfection [38]. For cell-cell fusion activity, hACE2-293T or Caco2 cells transfected with pQCXIP-BSR-GFP11 were prepared as target cells; HEK293T expressing the wild-type (WT) or chimera S proteins and pQCXIP-GFP1-10 were prepared as effector cells. In brief, the 293T cells were grown to 80% confluence in a 12-well plate and transfected with 1 µg pQCXIP-GFP1-10 and 1µg pcDNA3.1(+)-SARS2 S-FLAG (WT or chimera), the hACE2-293T or Caco2 cells in a 12-well plate were transfected with 1µg pQCXIP-BSR-GFP11. After 24h, the target cell and effector cell populations were washed and resuspended in DMEM 10% FBS, mixed at a 4:1 ratio in different

combinations, plated at 3x 10^5 cells per well in a 96-well plate, and the fluorescence images were taken at the indicated time point using a Zeiss LSM800 confocal laser scanning microscope and a Keyence all-in-one Fluorescence microscope BZ-X800. The GFP area was quantified on Image J, and the expression levels of surface S proteins were analyzed using FACS, and the GFP area was normalized to the mean fluorescence intensity (MFI) of surface S proteins, and the normalized values were shown as fusion activity.

Pseudotyped particles assay

HEK293T cells were transfected with 72 μg WT or chimera S plasmid into a 15 cm cell culture dish. After 24 h, the cells were washed twice and inoculated with VSV*△G-Luc at a multiplicity of infection of 0.1 for 1h. After the inoculum was removed, the cells were washed 5 times using PBS with 2% FPS and further cultured with a DMEM culture medium for 36h. The supernatant was harvested and centrifuged at 3000 rpm to free cellular debris, filtered through a 0.45 μm syringe filter, and stored at – 80°C in small aliquots.

To detect the neutralizing activity of antibodies, serial dilutions (1:3) of mAbs were mixed with an equal volume of 200 50% tissue culture infectious doses (TCID50) SARS2 and SARS VSVpp into a 96 well-plate and incubated for 1 h at 37 °C, and then ACE-293T cells (100 μl, 2 × 10^5 in DMEM) were added to all wells and incubated for further 24 h at 37 °C. Luciferase activity was analyzed by the luciferase assay system

(Promega). IC50 was determined by a four-parameter logistic regression using GraphPad Prism 8.0 (GraphPad Software Inc.)

Proteins and Monoclonal antibodies expression and purification

Proteins and antibodies were generated as described previously [67]. In brief, for S proteins and ACE2, target genes were firstly amplified and subcloned to pcDNA3.1(+) vetor, and after performing Site-Directed Mutagenesis, plasmids were transfected into HEK293T cells using polyethylenimine (PEI) and cultured for 5 days. The supernatant was collected and purified using Ni-sepharose. For antibodies, the single B cells of COVID19 convalescents were obtained and then sorted into 96-well plates, and the IgG heavy and light chain variable genes were amplified by reverse transcriptase polymerase chain reaction (RT-PCR) and cloned into human IgG1 expression vectors and co-transfected into HEK293T cells with equal amounts of heavy/light-chain plasmids. Five days post-transfection, the supernatants were collected and purified using protein A agarose beads.

Rescue and infection of recombinant SARS-CoV/SARS-CoV-2 virus

2×10^6 HEK293T cells were seeded in a 6-cm plate. After recovery for 24 h, HEK293T cells were transfected with three μg Rep (ref) and three μg plasmids encoding various S genes using Hieff TransTM Liposomal Transfection Reagent (Yeasen Biotech, Cat#40802ES03, Shanghai, China). Six h post-transfection, the medium containing the

480 mixture of DNA/transfection reagent was replaced with fresh medium. After recovery
481 for 36 to 48 h, the supernatants were collected for further use.

482 2×10^5 HEK293T-ACE2 cells were seeded in one well of a 6-well plate. After
483 recovery for 24 h, the HEK293T cells were infected with recombinant SARS-
484 CoV/SARS-CoV-2 viruses, and two h post-infection, the viruses-containing medium
485 was replaced with fresh medium. 24 h post-infection, the cells were collected for the
486 extraction of total RNA and/or protein.

487

488 Enzyme-linked immunosorbent assay (ELISA) to detect Spikes
489 binding ability to ACE2

490 ELISA was performed as described previously [67]. High-protein binding microtiter
491 plates (Costar) were coated with 2 μg/ml human ACE2 protein in PBS overnight at 4℃
492 respectively. After 3% BSA in PBS blocking, serially diluted S proteins 1:3 starting at
493 50 ng/μl were incubated for 1h at 37℃. After washing 6 times with PBST, a S2 antibody
494 from our lab, I24, was incubated at 10 μg/ml at 37℃ for 1h, after washing again, the
495 HPR-conjugated goat anti-human IgG antibody (Jackson Immuno Research, 1:2000)
496 was incubated for another 1h at 37℃. The plate was developed with Super Aquablue
497 ELISA substrate (eBiosciences). Absorbance was measured at 405 nm on a microplate
498 spectrophotometer (BioTek).

499

500 Effect of drug treatment on fusion ability and cell viability assay.

Camostat and E64d were diluted at different concentrations first and then added to the cell mixture for fusion assay in a 96-well plate. The cell mixture was then mixed gently and cultured in a 5% CO_2 environment at 37℃ for subsequent testing.

The effects of Camostat and E64d on cell viability were measured by CCK8 assay. 293T cells were seeded into a 96-well plate and were left untreated or treated with different concentrations of drugs for 24 h. After treatments, CCK8 was added into the culture medium and incubated for 1 h at 37 °C to measure the absorbance at 405 nm.

Phylogenetic analyses.

We selected representative sequences from the NCBI taxonomy *Sarbecovrius* grouping and compared them using mafft software. We then used fasttree software to construct a phylogenetic tree based on SARS-like S proteins.

Statistical analysis

The Prism software (Graphpad Version 8.0) was used for all statistical analyses. The significance of differences between the two groups was determined with a two-tailed Student's t-test. One-way or two-way analysis of variances with Bonferroni correction was employed for multi-group comparison. For all analyses, only a probability (*p*) value of 0.05 or lower were considered statistically significant (p > 0.05 [ns, not significant], p % 0.05 [*], p % 0.01 [**], p % 0.001 [***]).

Supporting information

S1 Fig. Reversing IFP motif of S2-chimera Spike influenced the fusogenicity significantly. (A and F) Schematic diagram of the S2 motif chimera Spike. The S2 was divided into 3 parts as Figure2 and to replace the corresponding area in turn. The F1 was further divided into two parts just as Figure2 did. The numbers in parentheses are identical to those in Figure3B-3E, 3F-3J. (B and G) Western blot. A representative blot of S-expressing cells (top) and quantified band intensity (the ratio of CL-S to the FL-S plus CL-S proteins) (bottom) are shown. (C and H) FACS. The summarized results of the surface S expression were shown. s309 antibody and mouse anti-human IgG-FITC were used respectively. (D and I) Spike-based fusion assay. The fusion activity was quantified by measuring the ratio of GFP+ area to DAPI area by imaging at different times (2, 6, 12 and 24hpt). The results for SARS2, Spike4, 15-19 or SARS, Spike2, 10-14 were shown as Saffron and grey lines, respectively. (E and J) Representative images of cell-cell fusion. Scale bar: 500 μm.

Results are means +/- SD from at least three fields per condition. Results are representative of at least three independent experiments. In B and G, statistically significant differences between parental S (Spike2 or Spike4) and chimeric Spikes were determined by a two-sided paired t test (*: $p<0.05$). In D and I, statistically significant differences between parental S (Spike2 or Spike4) and chimeric Spikes were determined by Student's test at each point (*: $p<0.05$，**: $p<0.01$).

S2 Fig. The Influence of TMPRSS2 on Spike fusogenicity. (A) Spike-based fusion assay. The fusion activity was quantified by measuring the ratio of GFP+ area to DAPI

545 area by imaging at different concentration of TMPRSS2 (0, 0.5, 1 and 2 μg). The results
546 for SARS2 and SARS were shown as Red and grey lines, respectively. (B)
547 Representative images of cell-cell fusion. Scale bar: 500 μm. (C) Western blot. A
548 representative blot of 293T cell lysates expressing TMPRSS2 with various
549 concentrations. Beta-actin was used as a control. (D) Cell viability assay. The cell
550 viability with different doses of Camostat and E64d was evaluated by CCK8 assay.

551 Results are means +/- SD from at least three fields per condition. Results are
552 representative of at least three independent experiments. Statistically significant
553 differences (**： $p<0.01$) between S813 Spike and T813 Spike were determined by
554 Student's test at each point (C, F and G).

555

556 **S3 Fig. Genomic description of AA 813 in Spike of *Sarbecovirus*.** (A) The
557 phylogenetic tree based on *Sarbecovirus* S proteins (SARS-like strains, n=24 genomes;
558 SARS strains, n=13 genomes; SARS2 strains, n=6 genomes). All strains invariantly
559 containing serine at position 813 were marked red while containing threonine were
560 marked mazarine. Color coding as indicated according to species. (B) Amino acid
561 frequency of site 813. 114 complete spike protein sequences of SARS were collected
562 from NCBI and 10,060,583 complete spike protein sequences of SARS2 (2020-2022)
563 were collected from GISAID. The method of analysis was performed as previously
564 described [69]. Briefly, After removing redundant sequences with 100% sequence
565 identity and multiple sequence alignment (MSA), site 813 based on the reference
566 sequence of SARS2 was derived and the amino acid frequency of site 813 can be

calculated based on the un-redundant dataset of SARS and SARS2, respectively. (C) Phylogenetic tree of Human coronavirus. The representative strains of 7 human coronaviruses were clustered by amino acid sequence phylogeny and observed the diversity of AA 813. In α-CoV (229E and NL63), there was only Alanine, while in β-CoV, Serine was in SARS2, MERS, OC34 and HKU1; threonine only in SARS. We used the WAG+F+I+G4 optimal model of the Iqtree software to construct a phylogenetic tree based on S proteins. The right-hand sequence mapping was based on texshade software for mapping. The secondary structure, i.e. the membrane fusion region, was predicted using the PSIPRED web page.

Acknowledgements

We would like to acknowledge Dr. Wenxia Tian at College of Veterinary Medicine, Shanxi Agricultural University for providing materials, technical support and valuable suggestions. We thank Dr Hai Li at School of Basic Medical Sciences, XI'AN JIAOTONG University for suggestions and revision of the manuscript.

Author Contributions

Conceptualization: Yong Ma, Yao-Qing Chen.

Data curation: Yong Ma, Tianyi Qiu, Pengbin Li.

Formal analysis: Yong Ma, Pengbin Li, Yunqi Hu.

Funding acquisition: Yao-Qing Chen, Yong Ma.

588 **Investigation:** Yong Ma, Pengbin Li, Yunqi Hu, Tianyi Qiu, Wenjing Zhao, Jun
589 Chen,Xiaoli Xiong, Mang Shi, Ji-An Pan3, Yao-Qing Chen

590 **Methodology:** Yong Ma, Pengbin Li, Yunqi Hu, Tianyi Qiu, Mang Shi, Jiaxin
591 Zhuang, Ji-An Pan.

592 **Project administration:** Yao-Qing Chen.

593 **Resources:** Hongjie Lu, Kexin Lv, Mengxin Xu, Jiaxin Zhuang, Xue Liu, Bing He,
594 Shuning Liu, Lin Liu, Yuanyuan Wang, Xinyu Yue, Yanmei Zhai, Wanyu Luo, Haoting
595 Mai, Jun Chen.

596 **Software:** Tianyi Qiu, Mang Shi.

597 **Supervision:** Yao-Qing Chen.

598 **Validation:** Yong Ma, Pengbin Li, Yunqi Hu.

599 **Visualization:** Yong Ma, Tianyi Qiu, Xue Liu, Lixiang Wang, Mang Shi.

600 **Writing – original draft:** Yong Ma, Pengbin Li.

601 **Writing – review & editing:** Yong Ma, Xiaoli Xiong, Mang Shi, Yao-Qing Chen.

602

603 **Fig 1. Replacement of S2 subunit affected the fusogenicity of S protein.** (A)
604 Schematic diagram for the construction of the S2-chimeric Spike. The Saffron graph
605 depicts SARS2 S, which has the multibasic motif (RRAR) at the S1/S2 Cleavage Site;
606 the grey graph represents SARS S. The numbers in parentheses are identical to those in
607 Figures 1B-1G. TM, transmembrane domain; CP, cytoplasmic domain. (B and C)
608 FACS. After transfection, the expression of surface S proteins was detected using s309
609 antibody which binds RBD efficiently and mouse anti-human IgG-FITC, respectively

(B) and the summarized results are shown (C). MFI, mean fluorescent intensity. (D) Western blot. Representative blots of cell lysates showing spike cleavage in parental and chimeric Spikes with or without trypsin treatment. Immunoblots were probed with anti-Flag tag Abs, the full-length (FL) and cleaved (CL) S protein were marked as indicated; Beta-actin was probed as a loading control. The band intensity was densitometrically calculated using Image J, and the ratio of Cleaved-S/total S (%) was shown. (E-G) Spike-based cell-cell fusion assay. A schematic diagram showing the GFP-split system for Spike-ACE2 mediated cell fusion (F), and representative images at 2, 12, 24, 48 h post-transfection (E). The summarized results of the ratio of fusion were shown (G). Scale bar, 500 μm.

Results are means +/- SD from at least three fields per condition. Results are representative of at least three independent experiments. Statistically significant differences between parental S (Spike1 or Spike3) and chimeric S (Spike2 or Spike4) were determined by a two-sided Student's t test (C and D, ns: non-significant), or two-sided paired t test (G, *: $p<0.05$，**: $p<0.01$).

Fig 2. Replacing IFP motif of parental Spike influenced the fusogenicity significantly. (A and G) Schematic diagram of the S2-chimeric Spike bearing swapped motif. The S2 was divided into 3 parts according to the structure and function: F1 (686-833), F2 (834-984) and F3 (985-1170) of SARS-CoV-2 (A); F1 (655-802), F2 (803-953), F3 (954-1182) of SARS-CoV (F). Then replacing the corresponding parts with the others separately. Further, the F1 was divided into two parts: FP (686-787) and IFP

(788-833) of SARS2 (A), or FP (655-756) and IFP (757-802) of SARS (F). The numbers in parentheses are identical to those in Figure 2B-2F, 2G-2L. (B and H) FACS. The summarized results of the surface S expression were shown. s309 antibody and mouse anti-human IgG-FITC were used respectively. (C, D and I, J) Western blot. A representative blot of cell lysates showing spike cleavage. FL-Spike and CL-Spike were marked as indicated. Beta-actin was used as a control. The band intensity was densitometrically calculated using Image J, and the ratio of Cleaved-S/total S (%) was shown. (E and K) Spike-based fusion assay. The fusion activity was quantified by measuring the ratio of GFP+ area to DAPI area by imaging at different times (2, 6, 12 and 24hpt). The results for SARS2, Spike4, 10-14 were shown as Saffron lines and SARS, Spike2, 5-9 were shown as grey lines, respectively. (F and L) Representative images of cell-cell fusion. Scale bar: 500 μm.

Results are means +/- SD from at least three fields per condition. Results are representative of at least three independent experiments. Statistically significant differences between parental S (Spike1 or Spike3) and chimeric Spikes were determined by two-sided paired t test (D and J, *: $p<0.05$, **： $p<0.01$), or Student's test at each point (E and K, *: $p<0.05$， **: $p<0.01$).

See also Figure S1.

Fig 3. S813T mutation affected the cell membrane fusion ability of IFP-chimeric Spike. (A and F) Schematic diagram of the IFP-chimeric Spike mutants and the numbers in parentheses are identical to those in Figure3B-3D and 3G-3I. Align the sequence of AA 788-833 in SARS2 with SARS (AA 770-815). Residue numbering is

shown according to SARS2 S. The mutation sites were marked in red or blue, and the S2' cleavage sites were in Green. (B and G) FACS. The summarized results of the surface S expression were shown. s309 antibody and mouse anti-human IgG-FITC were used respectively. (C and H) Western blot. Left panel: A representative blot of cell lysates from WT and mutant chimera-Spike expressing 293T cells, FL-Spike and CL-Spike were marked as indicated. Beta-actin was used as a control. Right panel: quantified band intensity using Image J to analyze the protein expression and the ratio of Cleaved-S to the total S. (D and I) Spike-based fusion assay. The fusion activity was quantified by measuring the ratio of GFP+ area to DAPI area by imaging at different times (2, 6, 12 and 24hpt). The results for mutant Spike9 and 14 were shown as yellow-green, Spike25-30 as blue lines, and Spike31-36 as red lines, respectively. (E and J) Representative images of cell-cell fusion. Scale bar: 200 μm.

Results are means +/- SD from at least three fields per condition. Results are representative of at least three independent experiments. Statistically significant differences between parental S (Spike9 or Spike14) and mutants were determined by Student's test at each point (D and I, *: $p<0.05$，**: $p<0.01$).

Fig 4. Spike S813T mutation disturbed the membrane fusion and infection of *Sarbecovirus* significantly. (A) Spike-based fusion assay. The fusion activity was quantified at different times (2, 6, 12 and 24hpt). ACE2-293T (Red) and Caco2 (Green) were used, the results of S813 Spike were shown as full lines and T813 Spike as dotted lines. (B) Representative images of cell-cell fusion. Scale bar: 200 μm. (C) FACS. The

676 summarized results of the surface S expression were shown. s309 antibody and mouse
677 anti-human IgG-FITC were used. S813 S and T813 S were shown as saffron and
678 magentas, respectively. (D) Western blot. Top panel: A representative blot of cell
679 lysates from S813 and T813 Spike expressing 293T cells, FL-Spike and CL-Spike were
680 marked as indicated. Beta-actin was used as a control. Bottom panel: quantified band
681 intensity using Image J to analyze the protein expression and the ratio of Cleaved-S to
682 the total S. (E) Pseudovirus assay. The replication of Pseudovirus with S813 or T813
683 Spike in ACE2-293T and Caco2 cells was determined by RT-qPCR, and the infectivity
684 percentage normalized with that of the virus pseudotyped with Spike1 was shown. S813
685 S and T813 S were shown as saffron and magentas, respectively.
686 Results are means +/- SD from at least three fields per condition. Results are
687 representative of at least three independent experiments. Statistically significant
688 differences (*: $p<0.05$) between S813 S and T813 S were determined by Student's test
689 at each point (A), or two-sided paired t test (D and E).
690
691 **Fig 5. The S813T mutation has no effect on S protein interactions with ACE2.** (A)
692 SDS-polyacrylamide gel electrophoresis (PAGE) of SARS2-6P, SARS-2P and Residue
693 813 substitution S variants. Molecular weight standards are indicated at the left in KD.
694 (B) Competitive ELSIA to detect the binding affinity between S proteins and ACE2.
695 Red line indicated SARS2, and blue line indicated SARS. (C) Neutralization curves for
696 RBD representative antibodies, m396 and X65, with the VSVpp containing parent and

mutant S proteins. Each point represents the mean and standard error of 2 independent measurements.

Fig 6. S813T mutation reduced the use of TMPRSS2 by S protein. (A) Schematic illustration of SARS S and SARS2 S including proteolytic cleavage sites: S1/S1, S2' and CTSL cleavage sites in S1. Residue 813 was indicated as red. Arrow heads indicated the cleavage site. (B) Western blot. Top panel: A representative blot of VSVpp digested with TPCK-trypsin (2 μg/ml at 37℃ for 30 min), FL-Spike (S) and CL-Spike (S2 and S2') were marked as indicated. Bottom panel: quantified band intensity using Image J to analyze the protein expression and the ratio of S2 and S2' to the total S. (C) Spike-based cell-cell fusion assay. With the overexpression of TMPRSS2 (purple) in ACE2-293T, the fusion activity was quantified at different times (2, 6, 12 and 24hpt). The results of S813 S were shown as full lines and T813 S as dotted lines. (D) Representative images of cell-cell fusion. The area of cell fusion was shown as green (up) and black (bottom). Scale bar: 500 μm. (E-G) Fusion inhibition of Camostat and E-64d in ACE2-293T+TMPRSS2. A schematic diagram showing the GFP-split system with the inhibitor Camostat and E-64d for Spike-ACE2/TMPRSS2 mediated cell fusion (E). After being pre-incubated with the indicated concentration (0, 10, 50, 100 μm) of Camostat (F) and E-64d (G), the fusion activity was quantified at different times (2, 6, 12 and 24hpt), and the results of Camostat were shown as purple and E-64d as blue.

Results are means +/- SD from at least three fields per condition. Results are representative of at least three independent experiments. Statistically significant

719 differences (*: $p<0.05$) between S813 Spike and T813 Spike were determined by
720 Student's test at each point (C, F and G).

721

722 References

723 **1.** Da Silva SJR, Do Nascimento JCF, Germano Mendes RP, Guarines KM,
724 Targino Alves Da Silva C, Da Silva PG, et al. Two Years into the COVID-19
725 Pandemic: Lessons Learned. ACS Infectious Diseases. 2022;8(9):1758-1814.

726 **2.** Dharmarajan G, Li R, Chanda E, Dean KR, Dirzo R, Jakobsen KS, et al. The
727 Animal Origin of Major Human Infectious Diseases: What Can Past Epidemics
728 Teach Us About Preventing the Next Pandemic? Zoonoses. 2022;2(1).

729 **3.** Zhou P, Yang XL, Wang XG, Hu B, Zhang L, Zhang W, et al. A pneumonia
730 outbreak associated with a new coronavirus of probable bat origin. Nature.
731 2020;579(7798):270-273.

732 **4.** Zhou P, Yang X-L, Wang X-G, Hu B, Zhang L, Zhang W, et al. A pneumonia
733 outbreak associated with a new coronavirus of probable bat origin. Nature.
734 2020;579(7798):270-273.

735 **5.** Cui J, Li F, Shi Z-L. Origin and evolution of pathogenic coronaviruses. Nature
736 Reviews Microbiology. 2019;17(3):181-192.

737 **6.** Stadler K, Masignani V, Eickmann M, Becker S, Abrignani S, Klenk H-D, et
738 al. SARS — beginning to understand a new virus. Nature Reviews
739 Microbiology. 2003;1(3):209-218.

740 **7.** Belouzard S, Millet JK, Licitra BN, Whittaker GR. Mechanisms of Coronavirus
741 Cell Entry Mediated by the Viral Spike Protein. Viruses. 2012;4(6):1011-1033.
742 **8.** Jackson CB, Farzan M, Chen B, Choe H. Mechanisms of SARS-CoV-2 entry
743 into cells. Nature Reviews Molecular Cell Biology. 2022;23(1):3-20.
744 **9.** Hoffmann M, Kleine-Weber H, Schroeder S, Krüger N, Herrler T, Erichsen S,
745 et al. SARS-CoV-2 Cell Entry Depends on ACE2 and TMPRSS2 and Is
746 Blocked by a Clinically Proven Protease Inhibitor. Cell. 2020;181(2):271-
747 280.e278.
748 **10.** Wang Q, Zhang Y, Wu L, Niu S, Song C, Zhang Z, et al. Structural and
749 Functional Basis of SARS-CoV-2 Entry by Using Human ACE2. Cell.
750 2020;181(4):894-904.e899.
751 **11.** Sun W, He L, Zhang H, Tian X, Bai Z, Sun L, et al. The self-assembled
752 nanoparticle-based trimeric RBD mRNA vaccine elicits robust and durable
753 protective immunity against SARS-CoV-2 in mice. Signal Transduct Target
754 Ther. 2021;6(1):340.
755 **12.** Yang S, Li Y, Dai L, Wang J, He P, Li C, et al. Safety and immunogenicity of
756 a recombinant tandem-repeat dimeric RBD-based protein subunit vaccine
757 (ZF2001) against COVID-19 in adults: two randomised, double-blind, placebo-
758 controlled, phase 1 and 2 trials. Lancet Infect Dis. 2021;21(8):1107-1119.
759 **13.** Zhang J, Hu Z, He J, Liao Y, Li Y, Pei R, et al. Safety and immunogenicity of
760 a recombinant interferon-armed RBD dimer vaccine (V-01) for COVID-19 in

761 healthy adults: a randomized, double-blind, placebo-controlled, Phase I trial.
762 Emerg Microbes Infect. 2021;10(1):1589-1597.
763 **14.** Barnes CO, Jette CA, Abernathy ME, Dam KA, Esswein SR, Gristick HB, et
764 al. SARS-CoV-2 neutralizing antibody structures inform therapeutic strategies.
765 Nature. 2020;588(7839):682-687.
766 **15.** He B, Liu S, Wang Y, Xu M, Cai W, Liu J, et al. Rapid isolation and immune
767 profiling of SARS-CoV-2 specific memory B cell in convalescent COVID-19
768 patients via LIBRA-seq. Signal Transduct Target Ther. 2021;6(1):195.
769 **16.** Cameroni E, Bowen JE, Rosen LE, Saliba C, Zepeda SK, Culap K, et al.
770 Broadly neutralizing antibodies overcome SARS-CoV-2 Omicron antigenic
771 shift. Nature. 2022;602(7898):664-670.
772 **17.** Deshpande A, Harris BD, Martinez-Sobrido L, Kobie JJ, Walter MR. Epitope
773 Classification and RBD Binding Properties of Neutralizing Antibodies Against
774 SARS-CoV-2 Variants of Concern. Front Immunol. 2021;12:691715.
775 **18.** Focosi D, Maggi F. Neutralising antibody escape of SARS-CoV-2 spike protein:
776 Risk assessment for antibody-based Covid-19 therapeutics and vaccines. Rev
777 Med Virol. 2021;31(6):e2231.
778 **19.** Greaney AJ, Starr TN, Barnes CO, Weisblum Y, Schmidt F, Caskey M, et al.
779 Mapping mutations to the SARS-CoV-2 RBD that escape binding by different
780 classes of antibodies. Nat Commun. 2021;12(1):4196.

781 **20.** Benton DJ, Wrobel AG, Xu P, Roustan C, Martin SR, Rosenthal PB, et al.
782 Receptor binding and priming of the spike protein of SARS-CoV-2 for
783 membrane fusion. Nature. 2020;588(7837):327-330.
784 **21.** Walls AC, Park YJ, Tortorici MA, Wall A, McGuire AT, Veesler D. Structure,
785 Function, and Antigenicity of the SARS-CoV-2 Spike Glycoprotein. Cell.
786 2020;181(2):281-292 e286.
787 **22.** Papa G, Mallery DL, Albecka A, Welch LG, Cattin-Ortolá J, Luptak J, et al.
788 Furin cleavage of SARS-CoV-2 Spike promotes but is not essential for infection
789 and cell-cell fusion. PLOS Pathogens. 2021;17(1):e1009246.
790 **23.** Tang T, Bidon M, Jaimes JA, Whittaker GR, Daniel S. Coronavirus membrane
791 fusion mechanism offers a potential target for antiviral development. Antiviral
792 Res. 2020;178:104792.
793 **24.** Yu S, Zheng X, Zhou B, Li J, Chen M, Deng R, et al. SARS-CoV-2 spike
794 engagement of ACE2 primes S2' site cleavage and fusion initiation. Proc Natl
795 Acad Sci U S A. 2022;119(1).
796 **25.** Iwata-Yoshikawa N, Okamura T, Shimizu Y, Hasegawa H, Takeda M, Nagata
797 N. TMPRSS2 Contributes to Virus Spread and Immunopathology in the
798 Airways of Murine Models after Coronavirus Infection. J Virol. 2019;93(6).
799 **26.** Zhao MM, Yang WL, Yang FY, Zhang L, Huang WJ, Hou W, et al. Cathepsin
800 L plays a key role in SARS-CoV-2 infection in humans and humanized mice
801 and is a promising target for new drug development. Signal Transduct Target
802 Ther. 2021;6(1):134.

803 **27.** Xia S, Liu M, Wang C, Xu W, Lan Q, Feng S, et al. Inhibition of SARS-CoV-
804 2 (previously 2019-nCoV) infection by a highly potent pan-coronavirus fusion
805 inhibitor targeting its spike protein that harbors a high capacity to mediate
806 membrane fusion. Cell Res. 2020;30(4):343-355.
807 **28.** Basso LGM, Zeraik AE, Felizatti AP, Costa-Filho AJ. Membranotropic and
808 biological activities of the membrane fusion peptides from SARS-CoV spike
809 glycoprotein: The importance of the complete internal fusion peptide domain.
810 Biochim Biophys Acta Biomembr. 2021;1863(11):183697.
811 **29.** Lai AL, Freed JH. Negatively charged residues in the membrane ordering
812 activity of SARS-CoV-1 and -2 fusion peptides. Biophys J. 2022;121(2):207-
813 227.
814 **30.** Santamaria A, Batchu KC, Matsarskaia O, Prévost SF, Russo D, Natali F, et al.
815 Strikingly Different Roles of SARS-CoV-2 Fusion Peptides Uncovered by
816 Neutron Scattering. J Am Chem Soc. 2022;144(7):2968-2979.
817 **31.** Coutard B, Valle C, de Lamballerie X, Canard B, Seidah NG, Decroly E. The
818 spike glycoprotein of the new coronavirus 2019-nCoV contains a furin-like
819 cleavage site absent in CoV of the same clade. Antiviral Res. 2020;176:104742.
820 **32.** Xu X, Chen P, Wang J, Feng J, Zhou H, Li X, et al. Evolution of the novel
821 coronavirus from the ongoing Wuhan outbreak and modeling of its spike protein
822 for risk of human transmission. Sci China Life Sci. 2020;63(3):457-460.

823 **33.** Shang J, Wan Y, Luo C, Ye G, Geng Q, Auerbach A, et al. Cell entry
824 mechanisms of SARS-CoV-2. Proc Natl Acad Sci U S A. 2020;117(21):11727-
825 11734.
826 **34.** Wrapp D, Wang N, Corbett KS, Goldsmith JA, Hsieh CL, Abiona O, et al. Cryo-
827 EM structure of the 2019-nCoV spike in the prefusion conformation. Science.
828 2020;367(6483):1260-1263.
829 **35.** Walls AC, Park YJ, Tortorici MA, Wall A, McGuire AT, Veesler D. Structure,
830 Function, and Antigenicity of the SARS-CoV-2 Spike Glycoprotein. Cell.
831 2020;181(2):281-292.e286.
832 **36.** Jackson CB, Farzan M, Chen B, Choe H. Mechanisms of SARS-CoV-2 entry
833 into cells. Nat Rev Mol Cell Biol. 2022;23(1):3-20.
834 **37.** Ren W, Ju X, Gong M, Lan J, Yu Y, Long Q, et al. Characterization of SARS-
835 CoV-2 Variants B.1.617.1 (Kappa), B.1.617.2 (Delta), and B.1.618 by Cell
836 Entry and Immune Evasion. mBio. 2022;13(2):e0009922.
837 **38.** Buchrieser J, Dufloo J, Hubert M, Monel B, Planas D, Rajah MM, et al.
838 Syncytia formation by SARS-CoV-2-infected cells. Embo j.
839 2020;39(23):e106267.
840 **39.** Rajah MM, Bernier A, Buchrieser J, Schwartz O. The Mechanism and
841 Consequences of SARS-CoV-2 Spike-Mediated Fusion and Syncytia
842 Formation. J Mol Biol. 2022;434(6):167280.

843 **40.** Schaub JM, Chou CW, Kuo HC, Javanmardi K, Hsieh CL, Goldsmith J, et al.
844 Expression and characterization of SARS-CoV-2 spike proteins. Nat Protoc.
845 2021;16(11):5339-5356.
846 **41.** Lu M, Chamblee M, Zhang Y, Ye C, Dravid P, Park JG, et al. SARS-CoV-2
847 prefusion spike protein stabilized by six rather than two prolines is more potent
848 for inducing antibodies that neutralize viral variants of concern. Proc Natl Acad
849 Sci U S A. 2022;119(35):e2110105119.
850 **42.** Hsieh CL, Goldsmith JA, Schaub JM, DiVenere AM, Kuo HC, Javanmardi K,
851 et al. Structure-based design of prefusion-stabilized SARS-CoV-2 spikes.
852 Science. 2020;369(6510):1501-1505.
853 **43.** Pallesen J, Wang N, Corbett KS, Wrapp D, Kirchdoerfer RN, Turner HL, et al.
854 Immunogenicity and structures of a rationally designed prefusion MERS-CoV
855 spike antigen. Proc Natl Acad Sci U S A. 2017;114(35):E7348-e7357.
856 **44.** Kirchdoerfer RN, Wang N, Pallesen J, Wrapp D, Turner HL, Cottrell CA, et al.
857 Stabilized coronavirus spikes are resistant to conformational changes induced
858 by receptor recognition or proteolysis. Sci Rep. 2018;8(1):15701.
859 **45.** Zhu Z, Chakraborti S, He Y, Roberts A, Sheahan T, Xiao X, et al. Potent cross-
860 reactive neutralization of SARS coronavirus isolates by human monoclonal
861 antibodies. Proc Natl Acad Sci U S A. 2007;104(29):12123-12128.
862 **46.** Li F. Structure, Function, and Evolution of Coronavirus Spike Proteins. Annu
863 Rev Virol. 2016;3(1):237-261.

47. Zhao MM, Zhu Y, Zhang L, Zhong G, Tai L, Liu S, et al. Novel cleavage sites identified in SARS-CoV-2 spike protein reveal mechanism for cathepsin L-facilitated viral infection and treatment strategies. Cell Discov. 2022;8(1):53.

48. Örd M, Faustova I, Loog M. The sequence at Spike S1/S2 site enables cleavage by furin and phospho-regulation in SARS-CoV2 but not in SARS-CoV1 or MERS-CoV. Sci Rep. 2020;10(1):16944.

49. Shang J, Ye G, Shi K, Wan Y, Luo C, Aihara H, et al. Structural basis of receptor recognition by SARS-CoV-2. Nature. 2020;581(7807):221-224.

50. Peacock TP, Goldhill DH, Zhou J, Baillon L, Frise R, Swann OC, et al. The furin cleavage site in the SARS-CoV-2 spike protein is required for transmission in ferrets. Nat Microbiol. 2021;6(7):899-909.

51. Lemmin T, Kalbermatter D, Harder D, Plattet P, Fotiadis D. Structures and dynamics of the novel S1/S2 protease cleavage site loop of the SARS-CoV-2 spike glycoprotein. J Struct Biol X. 2020;4:100038.

52. Lin JJ, Tien CF, Kuo YP, Lin EJ, Tsai WH, Chen MY, et al. Furin and TMPRSS2 Resistant Spike Induces Robust Humoral and Cellular Immunity Against SARS-CoV-2 Lethal Infection. Front Immunol. 2022;13:872047.

53. Hoffmann M, Kleine-Weber H, Schroeder S, Krüger N, Herrler T, Erichsen S, et al. SARS-CoV-2 Cell Entry Depends on ACE2 and TMPRSS2 and Is Blocked by a Clinically Proven Protease Inhibitor. Cell. 2020;181(2):271-280.e278.

885 **54.** Papa G, Mallery DL, Albecka A, Welch LG, Cattin-Ortolá J, Luptak J, et al.
886 Furin cleavage of SARS-CoV-2 Spike promotes but is not essential for infection
887 and cell-cell fusion. PLoS Pathog. 2021;17(1):e1009246.
888 **55.** Ou T, Mou H, Zhang L, Ojha A, Choe H, Farzan M. Hydroxychloroquine-
889 mediated inhibition of SARS-CoV-2 entry is attenuated by TMPRSS2. PLoS
890 Pathog. 2021;17(1):e1009212.
891 **56.** Braun E, Sauter D. Furin-mediated protein processing in infectious diseases and
892 cancer. Clin Transl Immunology. 2019;8(8):e1073.
893 **57.** Zhang Y, Zhang L, Wu J, Yu Y, Liu S, Li T, et al. A second functional furin
894 site in the SARS-CoV-2 spike protein. Emerg Microbes Infect. 2022;11(1):182-
895 194.
896 **58.** Muus C, Luecken MD, Eraslan G, Sikkema L, Waghray A, Heimberg G, et al.
897 Single-cell meta-analysis of SARS-CoV-2 entry genes across tissues and
898 demographics. Nat Med. 2021;27(3):546-559.
899 **59.** Simmons G, Gosalia DN, Rennekamp AJ, Reeves JD, Diamond SL, Bates P.
900 Inhibitors of cathepsin L prevent severe acute respiratory syndrome coronavirus
901 entry. Proc Natl Acad Sci U S A. 2005;102(33):11876-11881.
902 **60.** Huang IC, Bosch BJ, Li F, Li W, Lee KH, Ghiran S, et al. SARS coronavirus,
903 but not human coronavirus NL63, utilizes cathepsin L to infect ACE2-
904 expressing cells. J Biol Chem. 2006;281(6):3198-3203.

905 **61.** Kirtipal N, Bharadwaj S, Kang SG. From SARS to SARS-CoV-2, insights on
906 structure, pathogenicity and immunity aspects of pandemic human
907 coronaviruses. Infect Genet Evol. 2020;85:104502.
908 **62.** Korber B, Fischer WM, Gnanakaran S, Yoon H, Theiler J, Abfalterer W, et al.
909 Tracking Changes in SARS-CoV-2 Spike: Evidence that D614G Increases
910 Infectivity of the COVID-19 Virus. Cell. 2020;182(4):812-827.e819.
911 **63.** Mansbach RA, Chakraborty S, Nguyen K, Montefiori DC, Korber B,
912 Gnanakaran S. The SARS-CoV-2 Spike variant D614G favors an open
913 conformational state. Sci Adv. 2021;7(16).
914 **64.** Cheng YW, Chao TL, Li CL, Wang SH, Kao HC, Tsai YM, et al. D614G
915 Substitution of SARS-CoV-2 Spike Protein Increases Syncytium Formation and
916 Virus Titer via Enhanced Furin-Mediated Spike Cleavage. mBio.
917 2021;12(4):e0058721.
918 **65.** Pinto D, Park YJ, Beltramello M, Walls AC, Tortorici MA, Bianchi S, et al.
919 Cross-neutralization of SARS-CoV-2 by a human monoclonal SARS-CoV
920 antibody. Nature. 2020;583(7815):290-295.
921 **66.** Ma Y, Liang Y, Wang N, Cui L, Chen Z, Wu H, et al. Avian Flavivirus Infection
922 of Monocytes/Macrophages by Extensive Subversion of Host Antiviral Innate
923 Immune Responses. J Virol. 2019;93(22).
924 **67.** Chen YQ, Wohlbold TJ, Zheng NY, Huang M, Huang Y, Neu KE, et al.
925 Influenza Infection in Humans Induces Broadly Cross-Reactive and Protective
926 Neuraminidase-Reactive Antibodies. Cell. 2018;173(2):417-429.e410.

927 **68.** Jin YY, Lin H, Cao L, Wu WC, Ji Y, Du L, et al. A Convenient and Biosafe
928 Replicon with Accessory Genes of SARS-CoV-2 and Its Potential Application
929 in Antiviral Drug Discovery. Virol Sin. 2021;36(5):913-923.
930 **69.** Liu X, Guo L, Xu T, Lu X, Ma M, Sheng W, et al. A comprehensive
931 evolutionary and epidemiological characterization of insertion and deletion
932 mutations in SARS-CoV-2 genomes. Virus Evol. 2021;7(2):veab104.
933

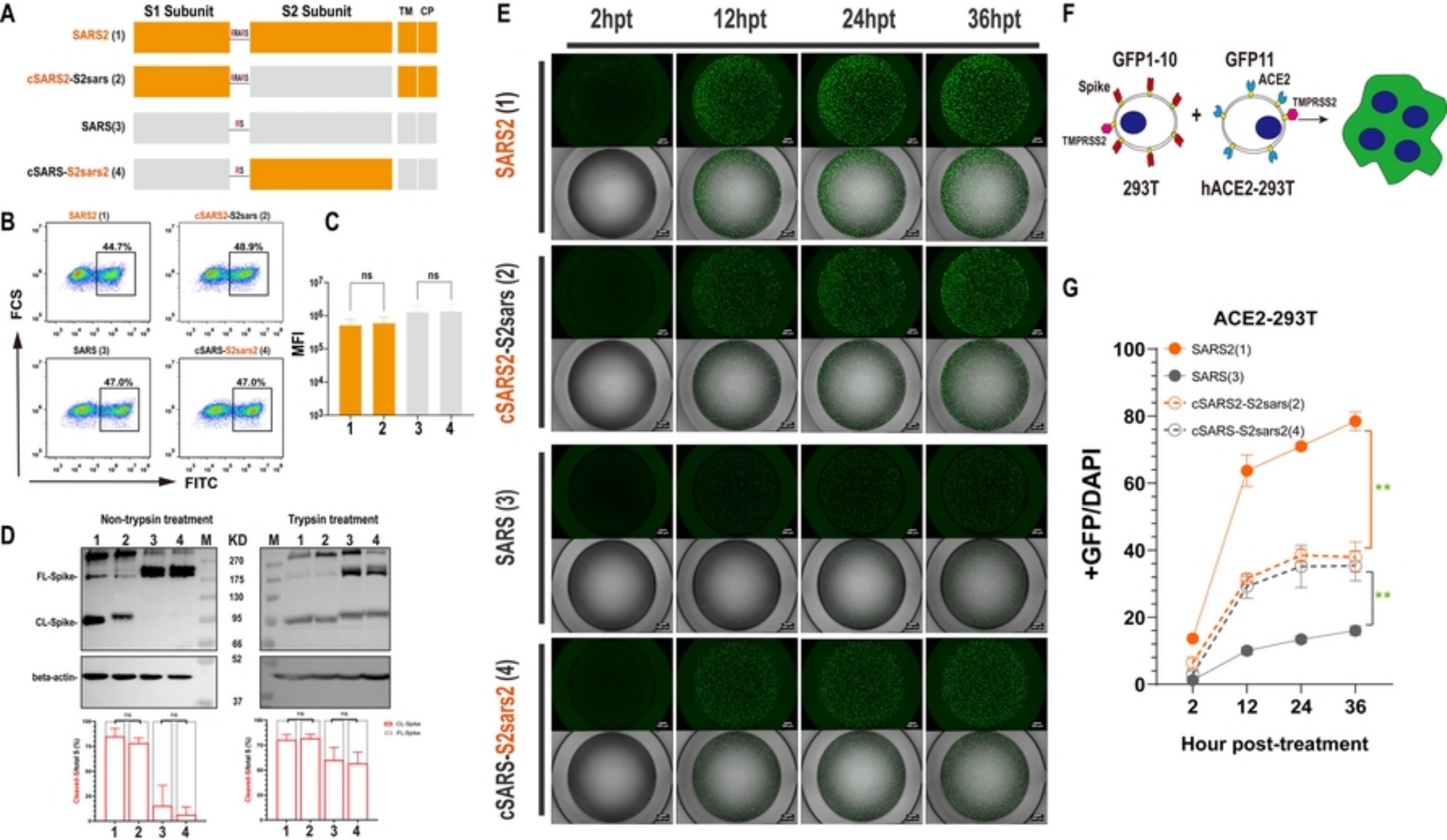
A
S1 Subunit
S2 Subunit
TM
CP
SARS2 (1)
RRAR
cSARS2-S2sars (2)
SARS(3)
RS
cSARS-S2sars2 (4)
B
SARS2 (1)
cSARS2-S2sars (2)
SARS (3)
cSARS-S2sars2 (4)
44.7%
48.9%
47.0%
47.0%
FCS
FITC
C
MFI
ns
ns
1
2
3
4
D
Non-trypsin treatment
Trypsin treatment
1 2 3 4 M
KD
M 1 2 3 4
270
175
130
95
66
52
37
FL-Spike-
CL-Spike-
beta-actin-
E
2hpt
12hpt
24hpt
36hpt
SARS2 (1)
cSARS2-S2sars (2)
SARS (3)
cSARS-S2sars2 (4)
F
GFP1-10
GFP11
Spike
ACE2
TMPRSS2
TMPRSS2
293T
hACE2-293T
G
ACE2-293T
SARS2(1)
SARS(3)
cSARS2-S2sars(2)
cSARS-S2sars2(4)
+GFP/DAPI
100
80
60
40
20
0
2
12
24
36
Hour post-treatment
**
**

Figure1

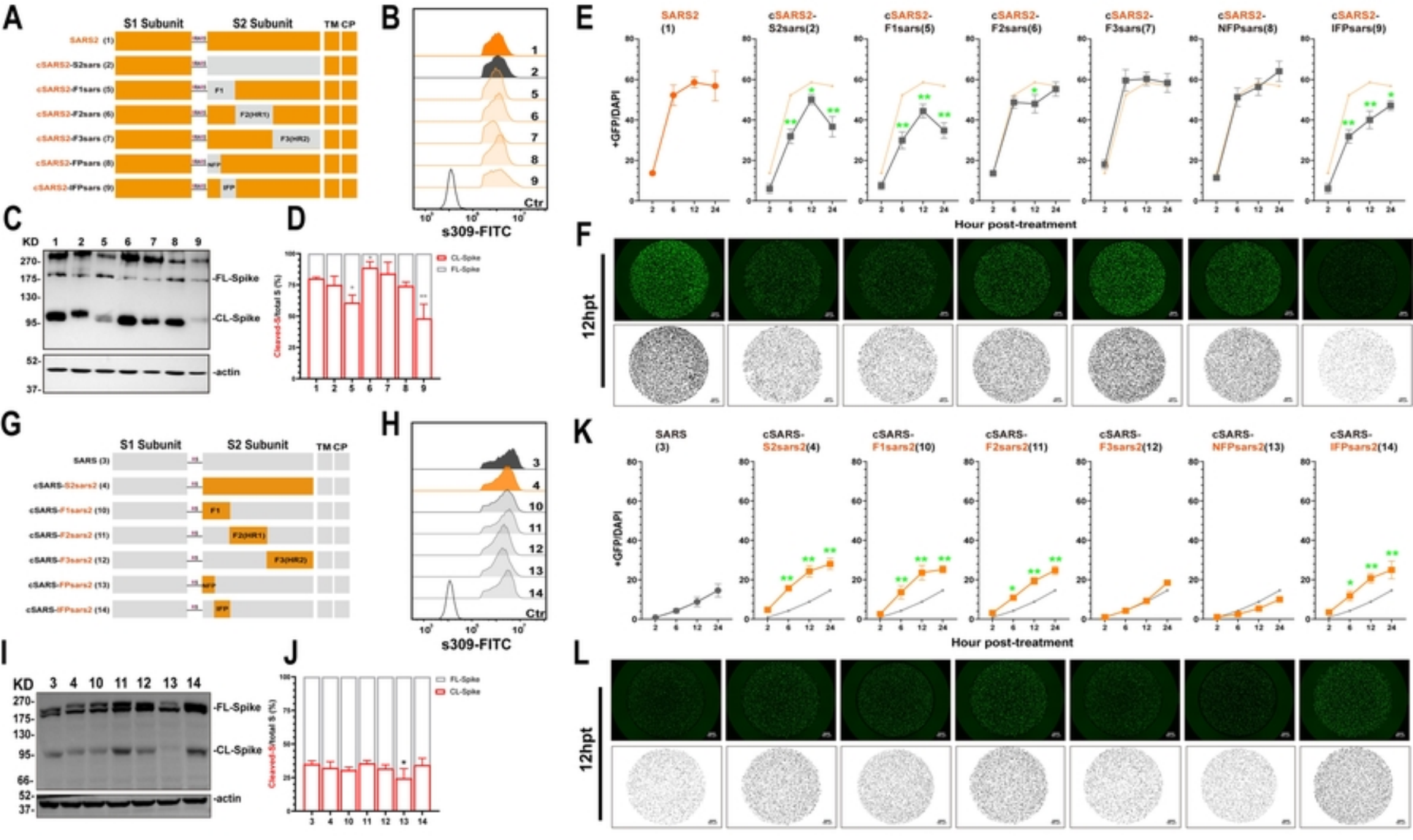
A
S1 Subunit
S2 Subunit
TM CP
SARS2 (1)
cSARS2-S2sars (2)
cSARS2-F1sars (5)
cSARS2-F2sars (6)
cSARS2-F3sars (7)
cSARS2-FPsars (8)
cSARS2-IFPsars (9)
F1
F2(HR1)
F3(HR2)
NFP
IFP
B
1
2
5
6
7
8
9
Ctr
s309-FITC
C
KD 1 2 5 6 7 8 9
270-
175-
130-
95-
52-
37-
-FL-Spike
-CL-Spike
-actin
D
Cleaved-S/total S (%)
CL-Spike
FL-Spike
1 2 5 6 7 8 9
E
SARS2 (1)
cSARS2-S2sars(2)
cSARS2-F1sars(5)
cSARS2-F2sars(6)
cSARS2-F3sars(7)
cSARS2-NFPsars(8)
cSARS2-IFPsars(9)
+GFP/DAPI
Hour post-treatment
F
12hpt
G
S1 Subunit
S2 Subunit
TM CP
SARS (3)
cSARS-S2sars2 (4)
cSARS-F1sars2 (10)
cSARS-F2sars2 (11)
cSARS-F3sars2 (12)
cSARS-FPsars2 (13)
cSARS-IFPsars2 (14)
F1
F2(HR1)
F3(HR2)
NFP
IFP
H
3
4
10
11
12
13
14
Ctr
s309-FITC
I
KD 3 4 10 11 12 13 14
270-
175-
130-
95-
66-
52-
37-
-FL-Spike
-CL-Spike
-actin
J
Cleaved-S/total S (%)
FL-Spike
CL-Spike
3 4 10 11 12 13 14
K
SARS (3)
cSARS-S2sars2(4)
cSARS-F1sars2(10)
cSARS-F2sars2(11)
cSARS-F3sars2(12)
cSARS-NFPsars2(13)
cSARS-IFPsars2(14)
+GFP/DAPI
Hour post-treatment
L
12hpt

Figure2

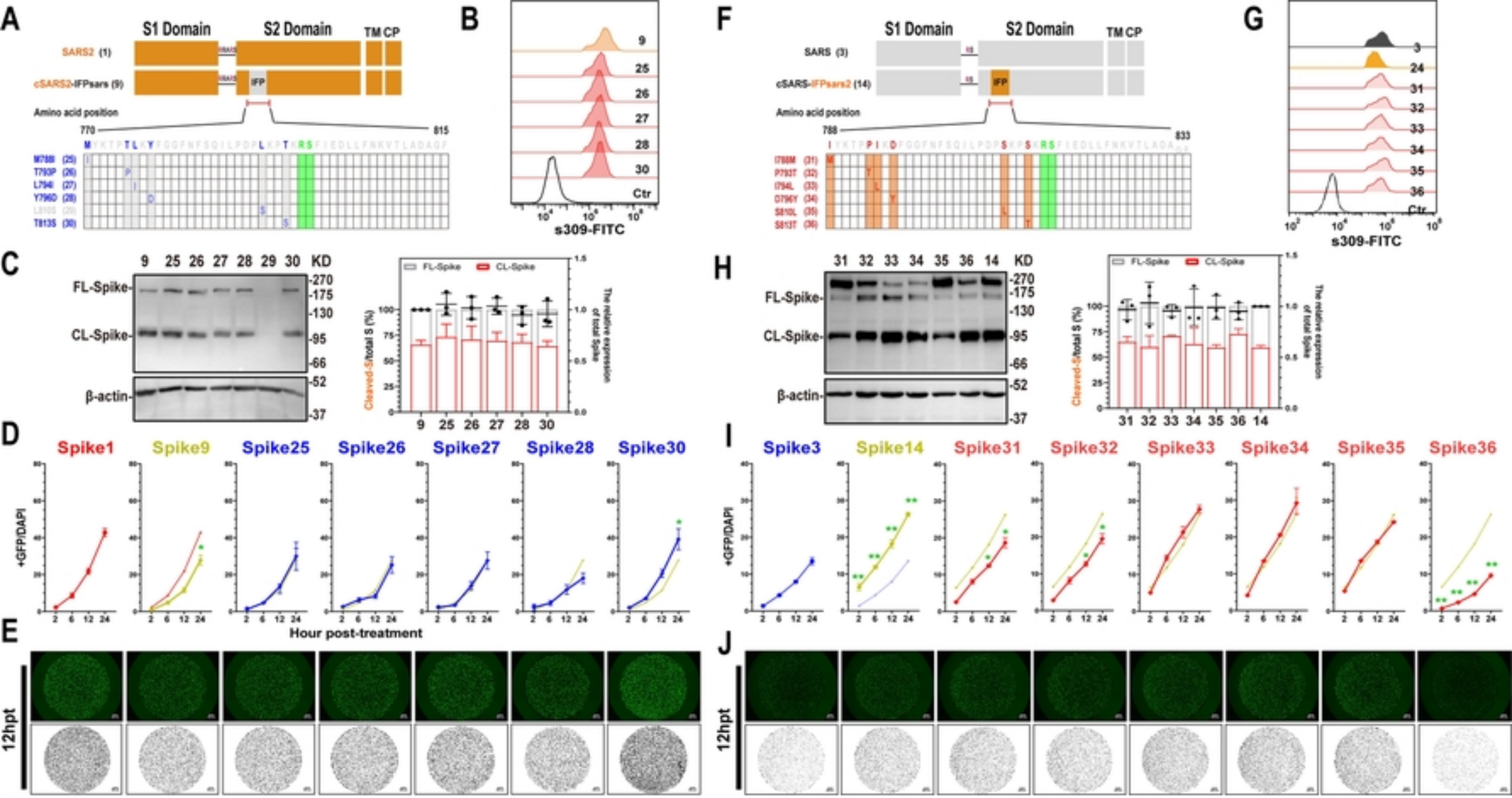
A
S1 Domain
S2 Domain
TM CP
SARS2 (1)
cSARS2-IFPsars (9)
IFP
Amino acid position
770
815
B
9
25
26
27
28
30
Ctr
s309-FITC
F
SARS (3)
cSARS-IFPsars2 (14)
788
833
G
3
24
31
32
33
34
35
36
C
9 25 26 27 28 29 30 KD
FL-Spike
CL-Spike
β-actin
270
175
130
95
66
52
37
FL-Spike
CL-Spike
Cleaved-S/total S (%)
The relative expression of total Spike
H
31 32 33 34 35 36 14 KD
D
Spike1
Spike9
Spike25
Spike26
Spike27
Spike28
Spike30
+GFP/DAPI
Hour post-treatment
I
Spike3
Spike14
Spike31
Spike32
Spike33
Spike34
Spike35
Spike36
E
12hpt
J

Figure3

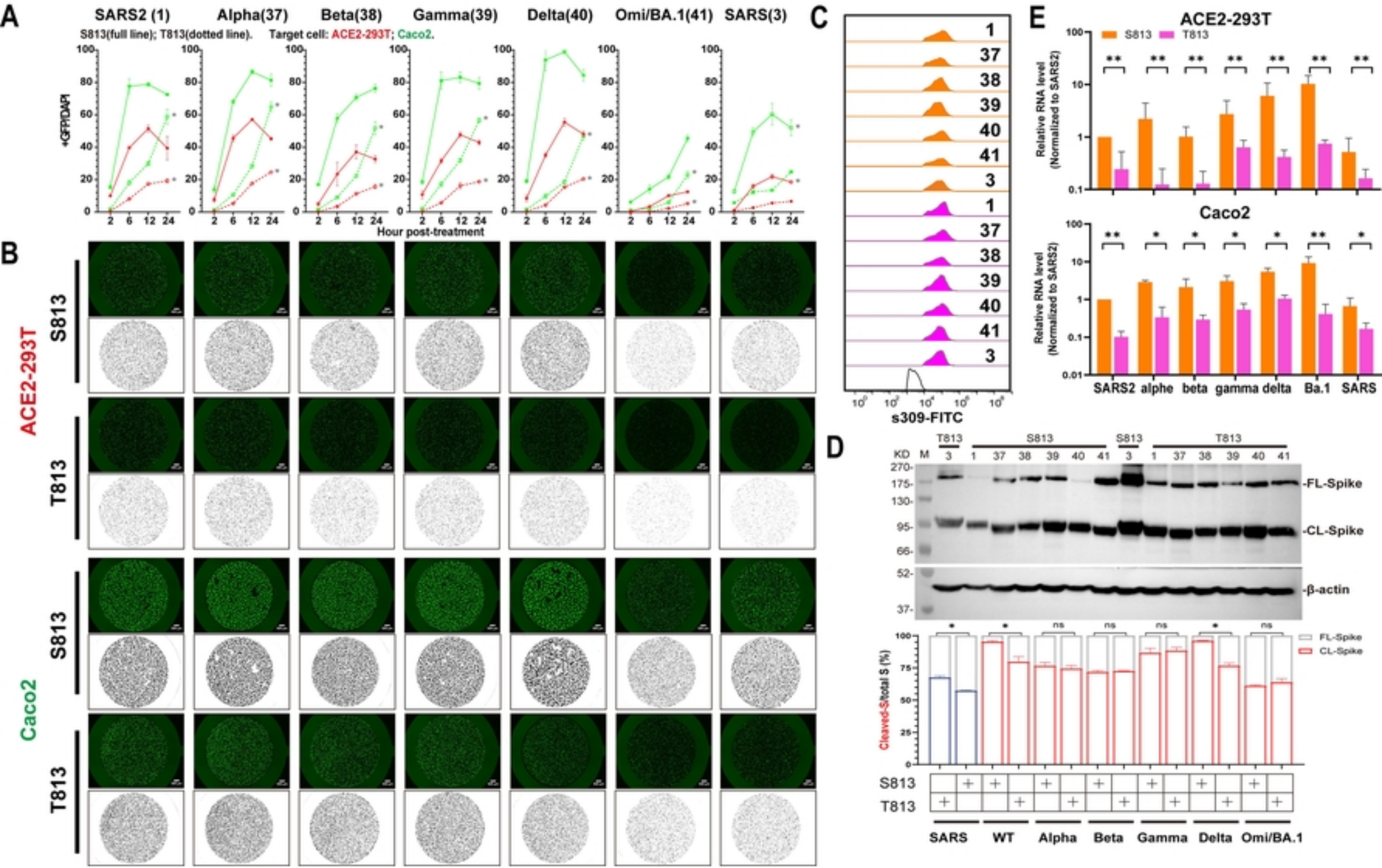
A
SARS2 (1)
Alpha(37)
Beta(38)
Gamma(39)
Delta(40)
Omi/BA.1(41)
SARS(3)
S813(full line); T813(dotted line).
Target cell: ACE2-293T; Caco2.
+GFP/DAPI
Hour post-treatment
B
ACE2-293T
Caco2
S813
T813
C
s309-FITC
D
KD
M
T813
S813
FL-Spike
CL-Spike
β-actin
Cleaved-S/total S (%)
SARS
WT
Alpha
Beta
Gamma
Delta
Omi/BA.1
E
ACE2-293T
Caco2
Relative RNA level (Normalized to SARS2)
SARS2
alphe
beta
gamma
delta
Ba.1
SARS

Figure4

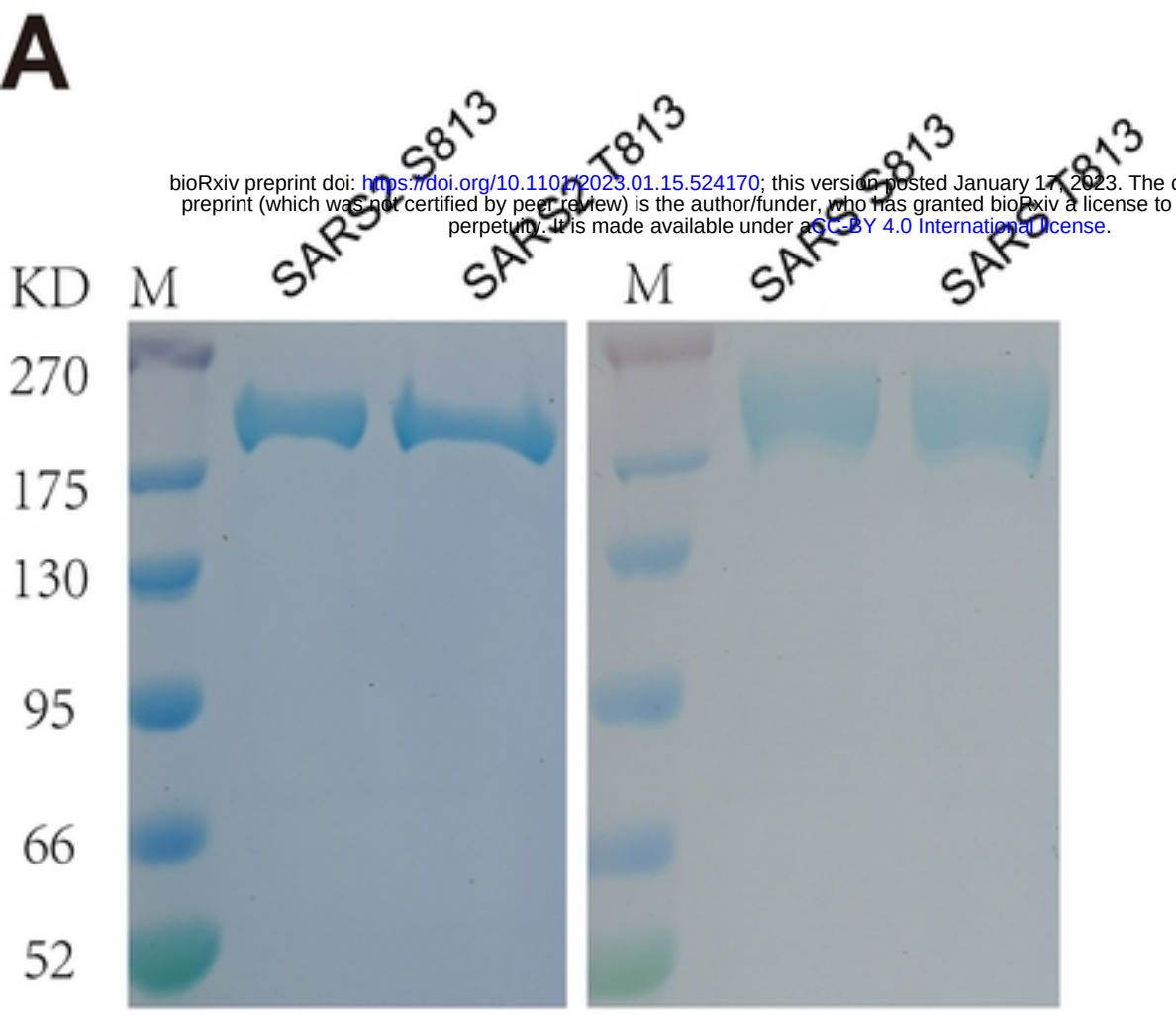

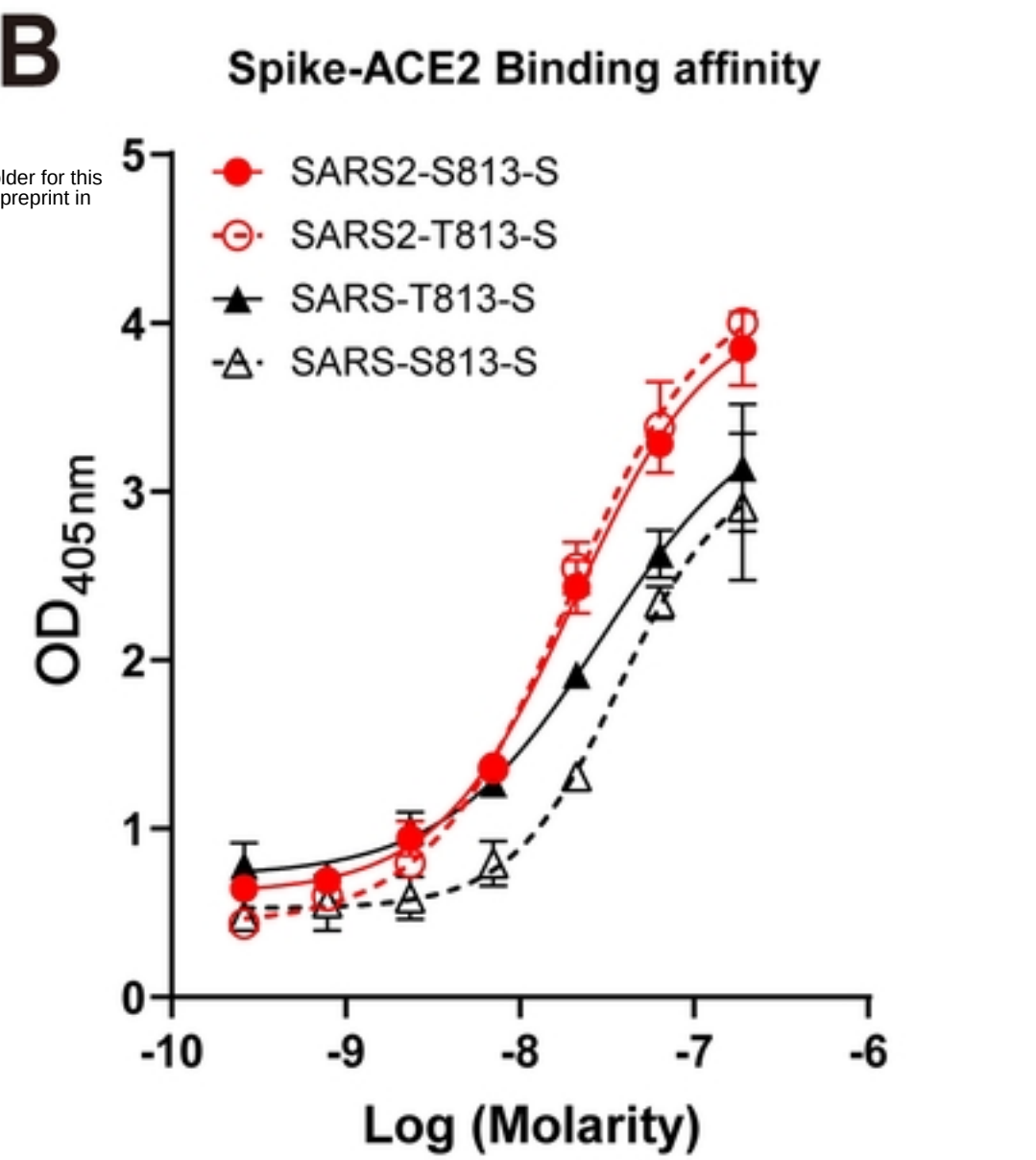

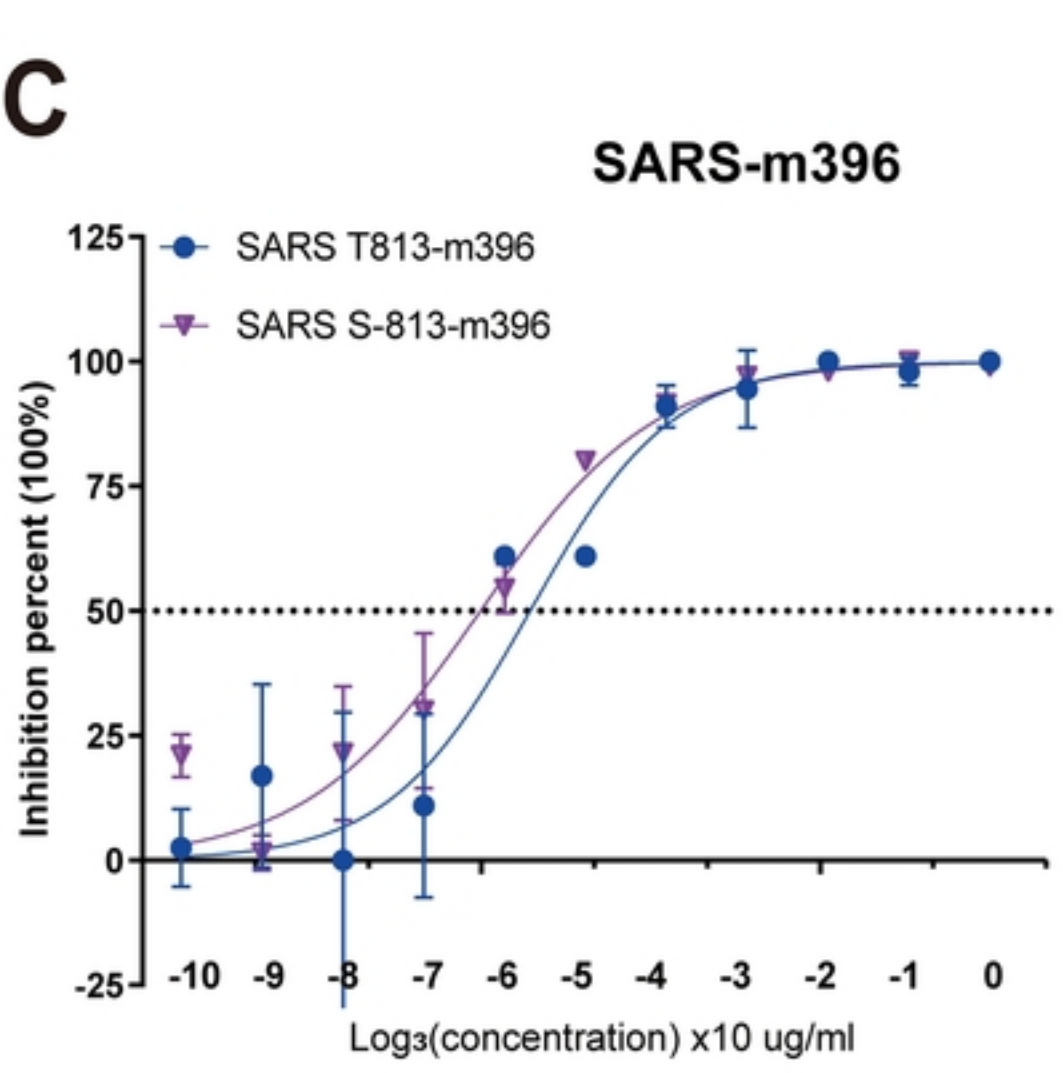

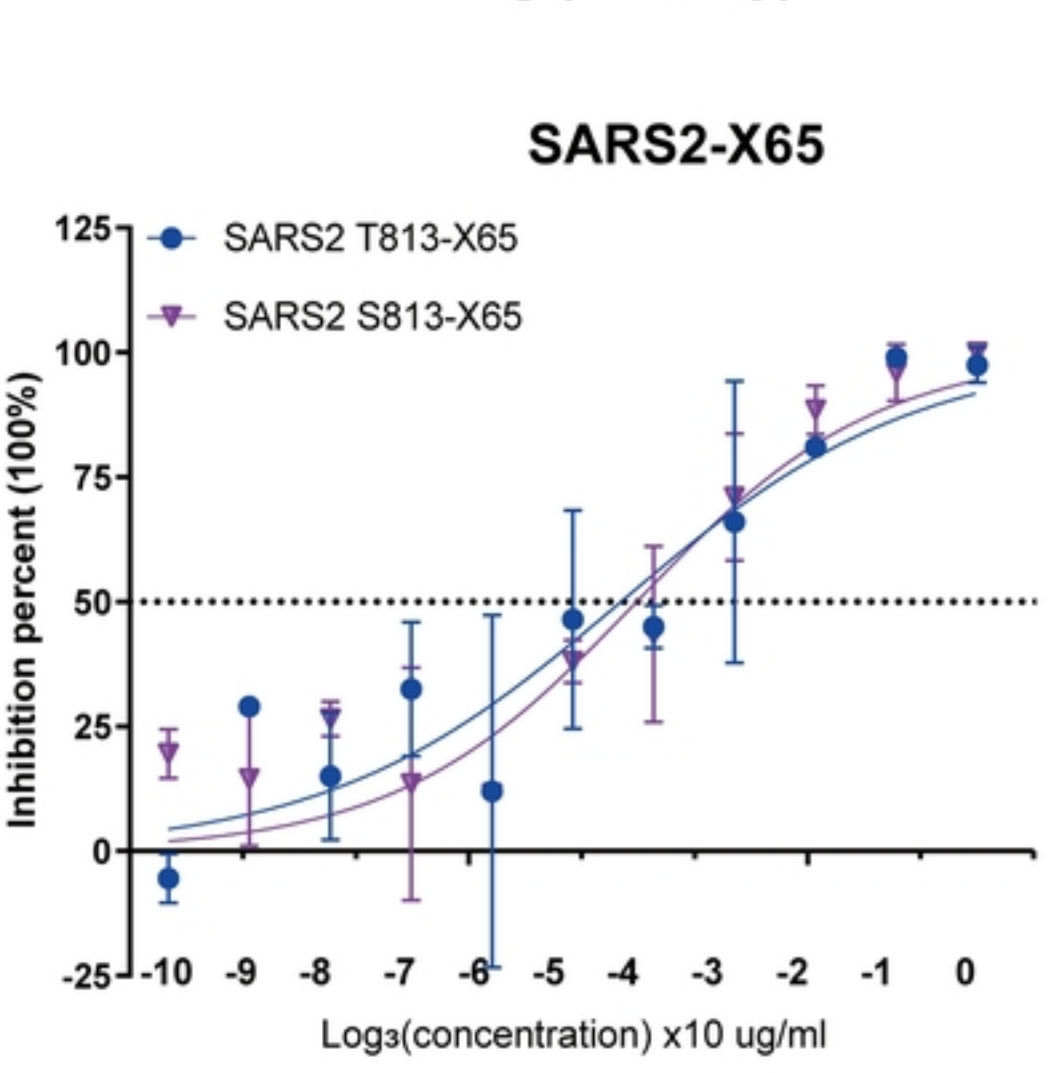

Figure5

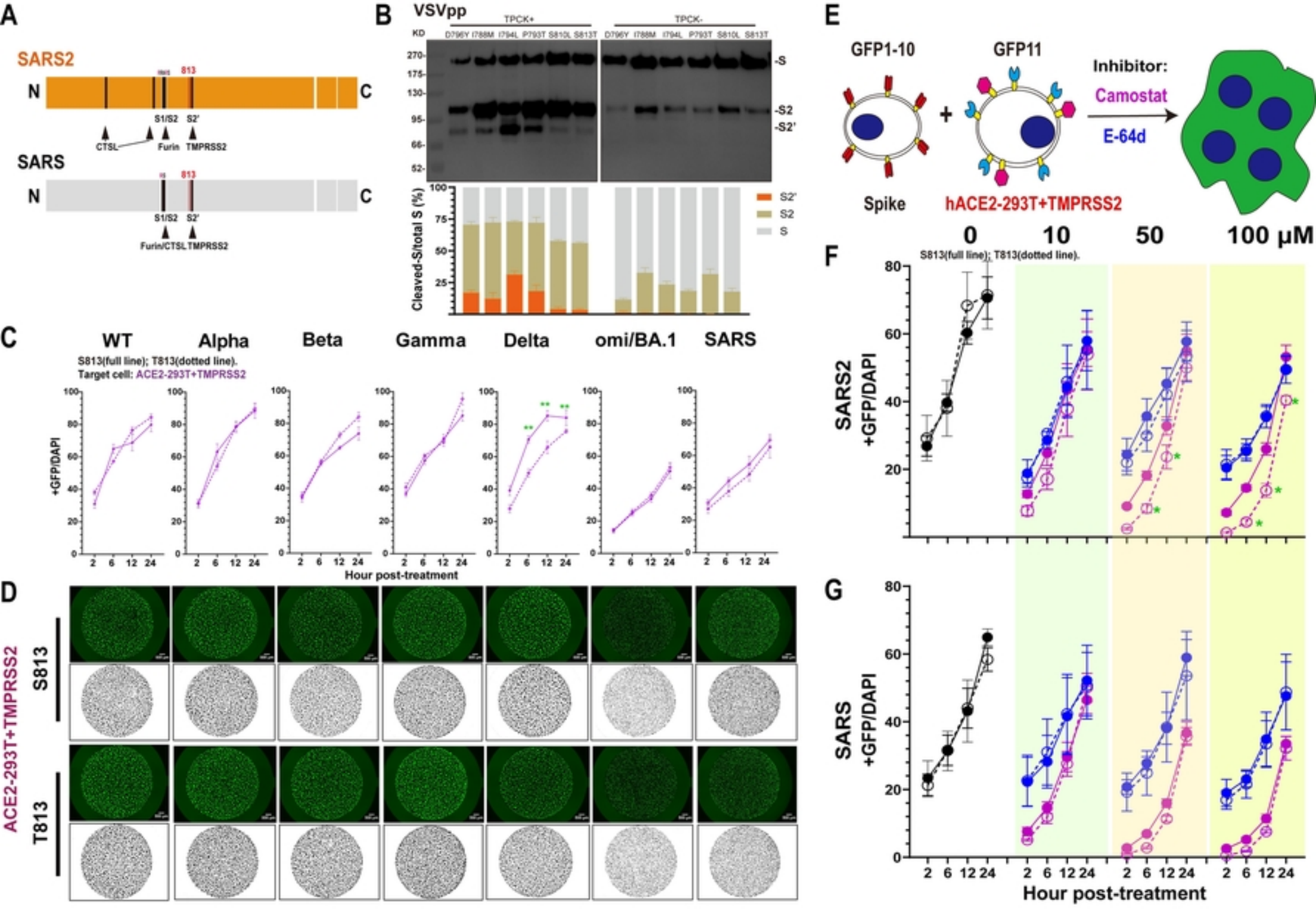
A
SARS2
N
C
S1/S2
S2'
CTSL
Furin
TMPRSS2
SARS
Furin/CTSL
B
VSVpp
TPCK+
TPCK-
KD
D796Y I788M I794L P793T S810L S813T
-S
-S2
-S2'
Cleaved-S/total S (%)
S2'
S2
S
C
WT
Alpha
Beta
Gamma
Delta
omi/BA.1
SARS
S813(full line); T813(dotted line).
Target cell: ACE2-293T+TMPRSS2
+GFP/DAPI
Hour post-treatment
D
S813
T813
ACE2-293T+TMPRSS2
E
GFP1-10
GFP11
Inhibitor:
Camostat
E-64d
Spike
hACE2-293T+TMPRSS2
0
10
50
100 μM
F
S813(full line); T813(dotted line).
SARS2
+GFP/DAPI
G
SARS
+GFP/DAPI
Hour post-treatment

Figure6

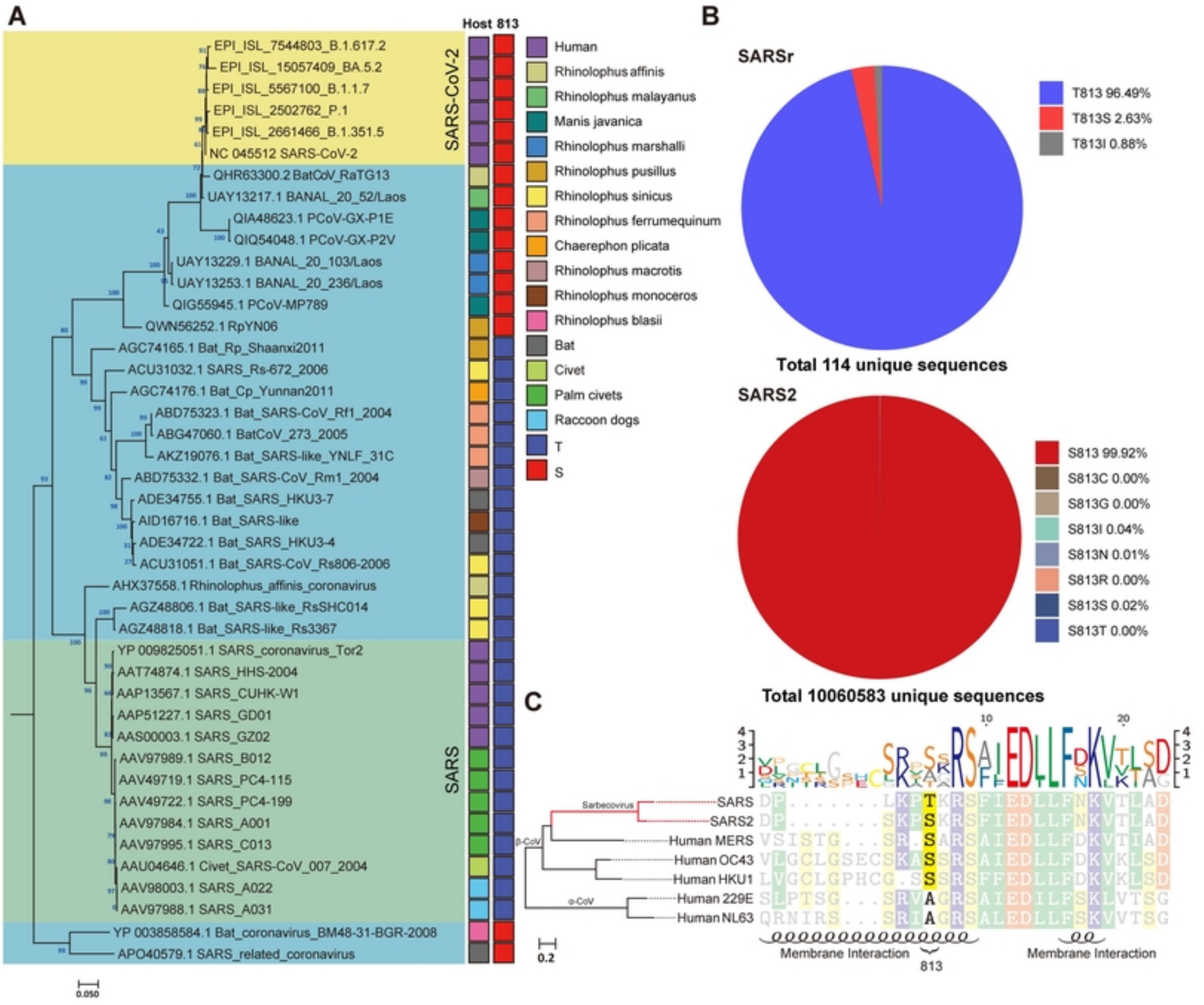

Figure7